On the nature of long range electronic coupling in a medium: Distance and orientational dependence for chromophores in molecular aggregates

Maximilian P. E. Lock, David L. Andrews, and Garth A. Jones

Articles you may be interested in

Assessment of mode-mixing and Herzberg-Teller effects on two-photon absorption and resonance hyper-Raman spectra from a time-dependent approach
J. Chem. Phys. **140**, 094107 (2014); 10.1063/1.4867273

Comparing the emissive dipole orientation of two similar phosphorescent green emitter molecules in highly efficient organic light-emitting diodes
Appl. Phys. Lett. **101**, 253304 (2012); 10.1063/1.4773188

Spectroscopic studies of the A − X electronic spectrum of the -hydroxyethylperoxy radical: Structure and dynamics
J. Chem. Phys. **135**, 184304 (2011); 10.1063/1.3656835

Theoretical investigation of the direct observation of anharmonic coupling in CDCl 3 in the time domain with femtosecond stimulated Raman scattering
J. Chem. Phys. **130**, 044312 (2009); 10.1063/1.3068709

Two-dimensional electronic spectra of symmetric dimers: Intermolecular coupling and conformational states
J. Chem. Phys. **124**, 124511 (2006); 10.1063/1.2180783

On the nature of long range electronic coupling in a medium: Distance and orientational dependence for chromophores in molecular aggregates

Maximilian P. E. Lock, David L. Andrews, and Garth A. Jones[a]
School of Chemistry, University of East Anglia, Norwich Research Park, Norwich, Norfolk NR4 7TJ, United Kingdom

The electronic coupling that mediates energy transfer in molecular aggregates is theoretically investigated using the principles of *quantum electrodynamics* (QED). In this context, both the electromagnetic tensor and rate equation relating to these couplings are re-examined with a focus on the role of the relative distance and orientation of transition dipole moment pairs, considering near-, intermediate-, and far-zone contributions to the coupling. The QED based coupling terms are investigated both analytically and numerically, and they are physically interpreted in terms of the character of the mediating (virtual) photons. The spatial dependence of the couplings for a two-dimensional molecular aggregate of ordered and isotropic transition dipole moments is numerically calculated. Further, *Pauli Master Equations* are employed for a one-dimensional chain of molecules and donor-acceptor pairs, to investigate the importance of intermediate- and far-zone contributions to the electronic coupling on electronic energy transfer dynamics. The results indicate that although Förster theory is often qualitatively and quantitatively correct for describing electronic energy transfer (EET) processes, intermediate- and far-zone coupling terms could sometimes be non-negligible for correctly describing EET in natural and artificial, mesoscopic, solar energy harvesting systems. In particular, the results indicate that these terms are non-negligible when using Förster resonance energy transfer spectroscopic ruler techniques for distances >10 nm. © *2014 AIP Publishing LLC.* [http://dx.doi.org/10.1063/1.4861695]

I. INTRODUCTION

Excitation energy transfer (EET), also known as resonance energy transfer (RET), is a process in which electronic energy may be transferred between molecular species.[1–4] Although the basic principles are well established and have been known for many years, there are still many open questions regarding the fundamental mechanisms of this inherently quantum mechanical phenomenon.

In many respects, the process of EET is well described by semiclassical theories of radiationless energy transfer, which generally assume the point-dipole approximation for the electronic coupling between the excitation donor and acceptor. EET events are, in this case, commonly considered as first order perturbative processes which are induced by the instantaneous Coulomb interaction. However, in reality, EET processes are fully quantum mechanical in nature and they are formally described within the framework of *quantum electrodynamics* (QED), where effects such as retardation must be taken into account.

Within the context of QED, both matter and radiation are treated quantum mechanically and they together constitute a closed quantum mechanical system. Here, the EET process is described by the coupling of an initially electronically excited donor to an acceptor which is initially in its ground state, via the photon vacuum field. QED provides accurate relations for the electronic coupling between the donor and acceptor chromophores which include *all* interactions over *all* distances. The energy transfer process emerges as a second-order process (signifying one light-matter interaction at the donor and one at the acceptor), mediated by the intermolecular propagation of virtual photons. When the donor and acceptor are part of a condensed phase system, the local electromagnetic fields arising from neighboring molecules "dress" the virtual photon fields, giving rise to virtual polaritons.

This approach to EET therefore requires finding the matrix element of the transition operator connecting the initial state (with the donor excited, and the acceptor and polariton fields in their respective ground states) with the final state (the acceptor being excited, and the donor and polariton fields in their ground states). The matrix element connecting the initial and final states of the system can be found using second order perturbation theory which includes intermediate states (to account for the time interval bounded by polariton creation and annihilation).[5] Within the framework of quantum dynamics, the matrix element is analogous to an off-diagonal coupling term appearing in the site basis Hamiltonian operator. The wavefunction or density matrix can then be evolved using the time-dependent Schrödinger equation or the Liouville von Neumann equation, respectively.[6] In the kinetics picture of EET, the modulus squared of the matrix element is the fundamental parameter that is used for

[a])garth.jones@uea.ac.uk

calculating the rate of energy transfer via the Fermi Golden Rule expression.[7]

In the case of energy transfer between molecular species beyond wavefunction overlap, there are two mechanistically distinct regimes of EET. The first is known as *radiationless* energy transfer and is often associated with the name of Förster.[8] Radiationless or *near-zone* energy transfer is characterized by an inverse sixth-power dependence of the rate on separation of the donor and acceptor chromophores, R^{-6}. This is the most dominant mechanism over short, non-contact distances. The latter mechanism, which occurs at longer ranges and is known as *radiative* energy transfer, was first addressed in the context of fluorescence reabsorption,[9] and subsequently recognized as *far-zone* transfer by Avery;[10] its rate obeys an inverse square law, R^{-2}. However, it is now known that within the framework of a unified theory of EET, these are both simply limits of a more general mechanism that operates over all distances.[11–13] Interestingly, this unified theory also predicts an intermediate range over which there is a mechanism that has both short and long range character: the rate of EET occurring in this intermediate range usually has an inverse fourth-power dependence, R^{-4}. Experimentally, this term proves difficult to identify, because it always occurs in conjunction with either the R^{-2} or the R^{-6} term or both. When EET occurs within the condensed phase, however, local field effects exerted through the molecular polarizability of the medium can result in refractive indices with a large imaginary component.[14] This gives rise to additional odd-powered terms, namely, R^{-3} and R^{-5}, when the matrix element is squared (Sec. II B).

Under suitable circumstances, such as when studying the phenomenon of EET over long distances (i.e., greater than the Förster radius – the separation at which the rate of energy transfer equates to that of spontaneous emission by the donor), these additional correction terms prove more amenable to experimental detection, as will be shown. In particular, within highly absorbing media the additional terms could become particularly important, for example, in molecular aggregate systems such as biological photosynthetic units where excitation may be transferred *between* antenna complexes,[15, 16] and also in optically active materials including J- and H-aggregates and quantum dot assemblies,[17–23] where the complex refractive index can have a large imaginary contribution. In these examples, EET may occur over tens or even hundreds of nanometers within a condensed phase environment. Of particular interest to this study is the distance and orientational dependence of a pair of chromophores (technically the dependence on their transition dipole moments (TDMs)), embedded within a condensed phase. Specifically the matrix element (cast in terms of the electromagnetic coupling tensor, *vide infra*) and its modulus squared considered analytically and numerically. In Sec. II of this paper, the background QED theory of EET in a vacuum and the condensed phase is reviewed along with the geometrical description of the electric fields associated with the mediating photons. In Sec. III, the results of the analytical and numerical studies of the electronic coupling terms are presented, and finally the conclusions and outlook are summarised in Sec. IV.

II. THEORY

A. QED formalism and EET in vacuum

The full QED description of the unified EET process can be found elsewhere.[5, 12] For convenience and completeness, important elements of the theory that are central to this study will be briefly outlined in this section.

For the case of a two-chromophore system, electronic energy transfer from a donor to an acceptor chromophore in the absence of a surrounding medium can be described by the Hamiltonian,

$$H = H_{\text{mol}}(D) + H_{\text{mol}}(A) + H_{\text{rad}} + H_{\text{int}}(A) + H_{\text{int}}(D), \quad (1)$$

where H_{rad} describes Hamiltonian for the radiation field,

$$H_{\text{rad}} = \sum_{\mathbf{k},\lambda} a^{(\lambda)\dagger}(\mathbf{k}) a^{(\lambda)}(\mathbf{k}) \hbar ck + e_{vac} \quad (2)$$

involving a sum over radiation modes with wave-vector $\mathbf{k}$ and polarization λ; the operators $a^{(\lambda)\dagger}(\mathbf{k})$ and $a^{(\lambda)}(\mathbf{k})$ are the creation and annihilation operators of a photon, respectively, and e_{vac} is the energy of the vacuum. In Eq. (1), $H_{\text{mol}}(X)$ is the usual molecular Hamiltonian for species X (=A, D, respectively, signifying the energy donor and acceptor) positioned at $\mathbf{R}_X$. The electronic coupling between chromophores occurs strictly through the interaction of the molecular sub-systems and the quantized field, i.e., there is no term in the Hamiltonian that directly couples the two chromophores. The dipole interaction Hamiltonian is given by

$$H_{\text{int}}(X) = -\varepsilon_0^{-1} \mu_\alpha(X) . \mathbf{d}_\alpha^\perp(\mathbf{R}_X), \quad (3)$$

where $\mu_\alpha(X)$ is the transition dipole moment between the electronic ground state and state α of chromophore X, and the electric displacement field operator is given by

$$\mathbf{d}^\perp(\mathbf{R}) = i \sum_{k,\lambda} \left(\frac{\hbar ck\varepsilon_0}{2V} \right)^{1/2} \mathbf{e}^{(\lambda)}(\mathbf{k})$$
$$\times \{ a^{(\lambda)}(\mathbf{k}) e^{i\mathbf{k}\cdot\mathbf{R}} - a^{(\lambda)\dagger}(\mathbf{k}) e^{-i\mathbf{k}\cdot\mathbf{R}} \}, \quad (4)$$

where $\mathbf{e}^{(\lambda)}(\mathbf{k})$; ($\lambda = 1, 2$) represents an orthogonal pair of polarization vectors, and V is the quantization volume.

Following standard QED procedures of using this Hamiltonian to calculate the matrix element connecting the initial and final states, one arrives at the EET rate equation, the Fermi Golden Rule,

$$W_{FI} = \frac{2\pi}{\hbar} |\langle F|\hat{T}|I\rangle|^2 \delta(E_I - E_F). \quad (5)$$

Here, $\hat{T}$ is the *transition operator* (taken to second order). The transition matrix element can be reformulated as

$$\langle F|T^{(2)}|I\rangle = \mu_{A_l}^{full} \theta_{lj}^{vac} \mu_{D_j}^{full}, \quad (6)$$

where

$$\boldsymbol{\mu}_D^{full} = \langle D|\boldsymbol{\mu}(D)|D^*\rangle, \quad \boldsymbol{\mu}_A^{full} = \langle A^*|\boldsymbol{\mu}(A)|A\rangle, \quad (7)$$

in which the superscript *full* indicates that both electronic and vibrational contributions are taken into account, and the final

form of the electromagnetic coupling tensor can be written as

$$\theta_{lj}^{vac}(k, \hat{\mathbf{R}}) = \frac{k^3 e^{iKR}}{4\pi\varepsilon_0}\left[(\delta_{lj} - 3\hat{R}_l\hat{R}_j)\left(\frac{1}{k^3 R^3} - \frac{i}{k^2 R^2}\right)\right.$$
$$\left. - (\delta_{lj} - \hat{R}_l\hat{R}_j)\frac{1}{kR}\right]. \quad (8)$$

In Eq. (8), and throughout this paper, the summation convention over the repeated Cartesian indices is applied. The subscripts l and j denote Cartesian components referring to the 3 spatial dimensions, k is the wavenumber corresponding to the transferred energy, R is the distance between chromophores, δ_{lj} is the Kronecker delta, and $\hat{\mathbf{R}}$ represents a unit vector parallel to the donor-acceptor separation vector. The retarded dipole-dipole coupling tensor, Eq. (8), displays the three regimes of energy transfer. The R^{-3} term is characteristic of nonradiative (near-zone) energy transfer, $kR \ll 1$, while the R^{-1} term corresponds to radiative (far-zone) transfer, $kR \gg 1$. The less familiar R^{-2} term is especially interesting, as it is expected to play an important role at critical retardation distances where $kR \sim 1$. This quasi-equality occurs when the distance between the donor and the acceptor is of the order of one sixth the wavelength of the mediating photon (specifically, the reduced wavelength, $\lambda = \lambda / 2\pi$).

Substituting the electromagnetic tensor, Eq. (8) into the rate equation (5), then after considerable manipulation including Born-Oppenheimer separation of the nuclear and electronic wavefunctions, and averaging over the initial and summing over the final states, we arrive at a rate equation in the following form:

$$W_{DA} = \frac{2\pi}{\hbar}\sum_{n,m,r,p}\rho_D^{(n)}\rho_A^{(m)}\left|\langle\varphi_D^{(r)}|\varphi_D^{(n)}\rangle\langle\varphi_A^{(p)}|\varphi_A^{(m)}\rangle\right|^2$$
$$\times \left|\mu_{Al}\mu_{Dj}\theta_{lj}^{vac}(k, \mathbf{R})\right|^2\delta\left(e_{D_n^*} + e_{A_m} - e_{D_r} - e_{A_p^*}\right), \quad (9)$$

where $\rho_D^{(n)}$ and $\rho_A^{(m)}$ are population distribution functions of the initial vibrational states of the donor and acceptor, respectively, with n and m being the vibrational indices. Substituting Eq. (8) into Eq. (9) and collecting terms allows one to express the rate equation in terms of overlap integrals between the donor and acceptor spectra. Writing the circular frequency as $\omega = ck$, gives

$$W_{DA} = \frac{9}{8\pi c^2 \tau_D}\int_0^\infty F_D^{vac}(\omega)\sigma_A^{vac}(\omega)\omega^2 g^{vac}(\omega; \mathbf{R})d\omega \quad (10)$$

with

$$g^{vac}(\omega, \mathbf{R}) = \eta_3^2\frac{c^6}{\omega^6 R^6} + (\eta_3^2 - 2\eta_1\eta_3)\frac{c^4}{\omega^4 R^4} + \eta_1^2\frac{c^2}{\omega^2 R^2}. \quad (11)$$

The functions $\sigma_A^{vac}(\omega)$ and $F_D^{vac}(\omega)$ are the absorption cross-section of the acceptor and the emission spectrum of the donor, respectively,[3,14] and the parameter τ_D is the radiative lifetime of the donor. Full details of these terms can be found in Chap. 2 of Ref. 3. The parameter $g^{vac}(\omega, \mathbf{R})$ in Eq. (11) – which, for the following analysis will be written in terms of the wave-vector, is analogous to the square of the coupling term, with the three different regimes of EET making a contribution to the overall rate. Notably, the rotationally averaged

result in this vacuum formulation has no cross-terms in odd powers of R.

Also in Eq. (11), the orientational factors, $\eta_q(q = 1, 3)$, describe the influence of the relative orientations of the transition dipole moments of the donor and acceptor chromophores, given by

$$\eta_q = (\hat{\boldsymbol{\mu}}_A \cdot \hat{\boldsymbol{\mu}}_D) - q(\hat{\mathbf{R}} \cdot \hat{\boldsymbol{\mu}}_A)(\hat{\mathbf{R}} \cdot \hat{\boldsymbol{\mu}}_D). \quad (12)$$

In the case of near-zone, Förster-type coupling, this factor become most favourable when the transition dipole moments are parallel (or anti-parallel) to one another and to the displacement vector. Note the origin of these orientational factors in the terms $(\delta_{lj} - 3\hat{R}_l\hat{R}_j)$ and $(\delta_{lj} - \hat{R}_l\hat{R}_j)$ of Eq. (8). For an in-depth discussion of orientational aspects of EET, see Chap. 4 of Ref. 3. Throughout this paper, $\theta_{lj}(k, \mathbf{R})$ type parameters shall be referred to as *electromagnetic tensor coupling terms*, and $g(k, \mathbf{R})$ type parameters as *rate equation coupling terms*. It is important to bear in mind that the two are related quadratically.

B. EET in the condensed phase

In order to properly describe the EET process within a condensed phase medium, the effects of the molecules comprising the medium must be incorporated into the Hamiltonian.[14] Consequently, the Hamiltonian for EET in a vacuum, Eq. (1), is rewritten to include a *polariton bath*. This represents a subsystem which includes both the quantized electromagnetic field and the molecules that constitute the medium surrounding the units specifically involved in energy transfer

$$H = H_{mol}(D) + H_{mol}(A) + H_{pol} + H_{int}(D) + H_{int}(A), \quad (13)$$

where the Hamiltonian for the polariton bath can be broken down as

$$H_{pol} = H_{rad} + \sum_{X \neq D, A}[H_{mol}(X) + H_{int}(X)]. \quad (14)$$

The replacement of H_{rad} with H_{pol} allows one to derive, after lengthy algebra, the *retarded dipole-dipole coupling tensor* for a donor-acceptor pair *in a medium*,

$$\theta_{lj}(k, \hat{\mathbf{R}}) = \frac{1}{n^2}\left(\frac{n^2 + 2}{3}\right)^2\theta_{lj}^{vac}(nk, \mathbf{R}), \quad (15)$$

where n is the complex scalar refractive index of the medium ($n = n' + in''$). Here n'', the imaginary part of the refractive index, manifests itself as an energy loss to the medium. Note, to save unnecessarily complicated expressions, the refractive index is assumed to be isotropic and it is written without explicit reference to its dependence on the optical frequency. The dispersion properties are important, nonetheless, and in the calculations that follow it will always be evaluated at the frequency (wavenumber) corresponding to the energy being transferred.

Starting with Eq. (9), and introducing $\theta_{lj}(k, \mathbf{R})$ in place of $\theta_{lj}^{vac}(k, \mathbf{R})$, the rate of donor-acceptor energy transfer in a

dissipative medium becomes

$$W_{DA} = \frac{9}{8\pi c^2 \tau_D} \int_0^\infty F_D(\omega)\sigma_A(\omega)\omega^2 g(\omega, \mathbf{R}) e^{-2n''\omega R/c} d\omega$$

(16)

with the coupling (cast in terms of the wavenumber) now given by

$$g(k, \mathbf{R}) = |n|^2 \left| \eta_3 \left[\left(\frac{1}{nkR}\right)^3 - i\left(\frac{1}{nkR}\right)^2 \right] - \eta_1 \left(\frac{1}{nkR}\right) \right|^2$$

$$= \frac{1}{|n|^4} \left\{ \eta_3^2 \frac{1}{k^6 R^6} + 2\eta_3^2 n'' \frac{1}{k^5 R^5} \right.$$

$$+ \left[\eta_3^2 |n|^2 - 2\eta_1\eta_3(n'^2 - n''^2) \right] \frac{1}{k^4 R^4}$$

$$\left. + 2\eta_1\eta_3 n'' |n|^2 \frac{1}{k^3 R^3} + \eta_1^2 |n|^4 \frac{1}{k^2 R^2} \right\}.$$

(17)

It is immediately clear that the existence of an imaginary part in the refractive index gives rise to two more terms in the coupling – namely, terms in the odd powers of distance, R^{-3} and R^{-5}. The terms, $\sigma_A(\omega)$ and $F_D(\omega)$ in Eq. (16), have also been corrected for the influence of the host medium and are now given explicitly by

$$\sigma_A(\omega) = \frac{1}{n'} \left| \frac{n^2 + 2}{3} \right|^2 \sigma_A^{vac}(\omega)$$

(18)

and

$$F_D(\omega) = n' \left| \frac{n^2 + 2}{3} \right|^2 F_D^{vac}.$$

(19)

Therefore, it should be emphasized that the dielectric influences of the medium affect the transfer rate in several ways. First, through the modification of the spectral functions $F_D(\omega)$ and $\sigma_A(\omega)$; second, through the coupling term $g(\omega, \mathbf{R})$, and finally through the introduction of a real and negative contribution to the exponent in the exponential term, reflecting losses in an absorbing medium (in accordance with the Beer-Lambert Law). The inclusion of these factors is vital for the correct description of long range excitation energy transfer in a condensed phase medium.

C. The nature of the mediating photon in EET

Deep within the theory of quantum electrodynamics, interactions between electrons occur by the exchange of virtual photons. These are photons that emerge from and retreat into the vacuum; they are not detected because, following their release, they are almost immediately reabsorbed. The summation over all possible modes, for such virtual photons, leads by well-trodden paths to the detailed form of the electromagnetic coupling tensor, given in Eq. (8). It is important to note that the effective character of the photon in the near-zone ($R \leq \lambda/2\pi$, or $kR \leq 1$) is significantly different from that in the far-zone. We can understand this as follows.

Using the Helmholtz theorem, any vector fields can be separated into zero-curl (irrotational) and zero divergence (solenoidal) components

$$\mathbf{F}(\mathbf{R}) = \mathbf{F}^{Sol}(\mathbf{R}) + \mathbf{F}^{Irr}(\mathbf{R}),$$

(20)

where

$$\nabla \cdot \mathbf{F}^{Sol}(\mathbf{R}) = 0,$$

(21)

$$\nabla \times \mathbf{F}^{Irr}(\mathbf{R}) = 0,$$

(22)

and $\mathbf{F}(\mathbf{R})$ represents a generalized field.[24,25] When dealing with slowly moving (i.e., non-relativistic) particles in bound states, it is most useful to employ the *Coulomb gauge* when describing electromagnetic fields,[25,26] and in this case the irrotational parts of the electric and magnetic fields disappear field. (Indeed, the non-zero curls of these fields can be used as an alternative basis for representing electromagnetic properties.)[27] The result of the transversality associated with Eq. (21) is that for each electromagnetic mode, the electric and magnetic field vectors are disposed orthogonally to $\mathbf{k}$, the propagation vector. However, the *observed* behavior is not quite so straightforward, because differences emerge between the features of near- and far-field (respectively, short range and long range) coupling. In quantum electrodynamical terms, this can be understood as reflecting the fact that when the released photon is still close to the emitter, its short path renders it strongly subject to quantum uncertainty in vector momentum, crucially including direction. The upshot is that, when due summation is taken over all photon modes, consistent with the unobserved, virtual character of these photons, the near-field reveals not only components that are transverse, but also some components that are longitudinal *with respect to the displacement vector* $\mathbf{R}$ (Refs. 5 and 21). However, over longer distances the longitudinal component drops away until the behavior is consistent with a fully transverse field. In the far-field where remote detection can be made, the result is fully transverse fields, as are normally associated with real photons.

These features have important implications when distinguishing between the character of near- and far-zone EET. In general, one can envisage two opposing extremities. In the far-zone extreme, the photons have field components that are almost exclusively transverse with respect to $\mathbf{R}$, and which also oscillate perpendicular to the direction of propagation, $\hat{k}$. In the other limiting case, the net effect of summing a range of the photon field components in the near-zone is that the coupling acquires some longitudinal character with respect to $\mathbf{R}$, consistent with oscillations parallel to the displacement vector $\mathbf{R}$. The latter extreme allows for the coupling of two transition dipole moments that are parallel to one another and also *parallel to the displacement vector* (Fig. 1(a)), while transverse electric fields are able to couple transition dipole moments that are parallel to one another, but *perpendicular to the displacement vector* (Fig. 1(b)). Relative transition dipole moment orientations that are between these two extremes are coupled by both transverse and longitudinal field components, with the latter primarily featuring in the near-zone.[28] These features acquire particular importance when analysing near-zone and far-zone EET in terms of the coupling equations (15) and (17).
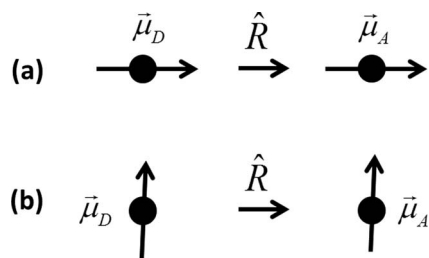
FIG. 1. EET is mediated by virtual photons. The photons have partial longitudinal electric field character in the near-zone and almost fully transverse electric field character in the far-zone. Longitudinal electric fields couple transition dipole moments with relative orientations as shown in (a), whereas transverse electric fields couple transition dipole moments with relative orientations, as shown in (b).

At the source (i.e., near the donor molecule) the electric field will be almost exclusively longitudinal and hence transition dipole moments arranged as shown in Fig. 1(a) will be strongly coupled in the near-zone. However, as the photon moves away from its source its associated electric field will take on a more transverse character and as it moves into the far-zone region it can couple transition dipole moments that are arranged as shown in Fig. 1(b).

III. RESULTS AND ANALYSIS

It is informative to consider in more detail the spatial dependence of both the electromagnetic coupling tensor, $\theta_{lj}(k, \mathbf{R})$, and rate equation coupling, $g(k, \mathbf{R})$, Eqs. (15) and (17), respectively. Each will be considered in turn. Of particular interest is how these parameters are affected by changes in chromophore separation and orientation. It is intuitively clear how the individual terms that comprise $\theta_{lj}(k, \mathbf{R})$ and $g(k, \mathbf{R})$ *qualitatively* depend on separation of the chromophores. However, the role of the relative orientation of the donor and acceptor on the coupling and transfer rate is less obvious.

In Sec. III A, the distance and orientation factors are considered both analytically and numerically. The numerical calculations are based on a uniformly distributed 2D grid of molecules of dimension 100 nm × 100 nm. The spatial variation of the electronic coupling between the donor and acceptor $V_{DA}^{QED} = \langle D|T^{(2)}|A \rangle = \mu_{D_l}^{full}\theta_{lj}\mu_{A_j}^{full}$, and also $g(k, \mathbf{R})$, are calculated between the central chromophore and all of the other chromophores comprising the 2D grid. Details of the numerical calculations are given in a subsequent section. It is important to point out that higher order effects are not considered in this study. That is, the effects of EET being assisted by ancillary molecules are not considered, as has been investigated previously for donor-mediator-acceptor systems.[29–31]

Finally, population dynamics for a series of one-dimensional (1D) molecular lattices and donor acceptor systems is investigated, by numerical integration of the *Pauli Master Equations* (PME). The purpose of this study is to determine how the population dynamics associated with rate constants derived from the R^{-6} dependent Förster coupling compares to that of the full, QED derived coupling, Eq. (17).

A. Orientation factors

The orientational factors, Eq. (12), is central to the energy transfer process. Comprehensive analyses of the standard near-field orientation factor (the rate dependence on "kappa squared," where κ signifies η_3 in our terminology) have been undertaken previously.[2] However, the broader perspective of the present analysis – no longer limited to short-range interactions – invites a revisitation of the orientation dependence, for comparison to the numerical results. In the analysis of long range energy transfer within a molecular aggregate, it will be beneficial to identify and analyse the various contributory factors. The orientation of the donor and acceptor, and their individual orientations with respect to their relative displacement vector, influence the terms in Eq. (17) in a variety of different ways. For example, the short range R^{-6} term is scaled by η_3^2, the intermediate range R^{-4} term is scaled by $(\eta_3^2 - 2\eta_1\eta_3)$ and the long range R^{-2} term is scaled by η_1^2. As the vectors in the orientational factor, Eq. (12) are of unit length, the expression can be rewritten in terms of cosine functions as

$$\eta_q = \cos(\phi_T) - q\cos(\phi_D)\cos(\phi_A), \tag{23}$$

where the angles are defined in Fig. 2.

The influence of the extreme values of each of the angles on the rate equation coupling term $g(k, \mathbf{R})$, is now considered. As a demonstration of limiting forms of behavior, the orientation factors, η_1^2, $\eta_1\eta_3$, η_3^2 are considered where ϕ_D, ϕ_A, and ϕ_T take possible values $\phi = 0$, $\phi = \pi/2$, and $\phi = \pi$. If all of the angles were independent of each other, this would lead to $3^3 = 27$ different cases to be considered. However, although there are four independent internal degrees of freedom for the transition dipole orientations in the donor-acceptor system, the angles ϕ_D, ϕ_A, and ϕ_T are not three of those; these angles are dependent on one another. For example, in cases where the transition dipole moments are parallel, then in order for the energy transfer to occur the separation vector is clearly prohibited from being parallel to one while at the same time orthogonal to the other. This dependence means that there are 10 special cases, of which 6 are unique. Moreover, since the orientation factors in Eq. (17) appear as η_1^2, $\eta_1\eta_3$, and η_3^2, then (η_1, η_3) leads to the same result as $(-\eta_1, -\eta_3)$; this results in only 2 unique cases, ignoring the trivial case where $(\eta_1, \eta_3) = (0, 0)$, which corresponds to forbidden energy transfer. Consequently, the two most interesting and
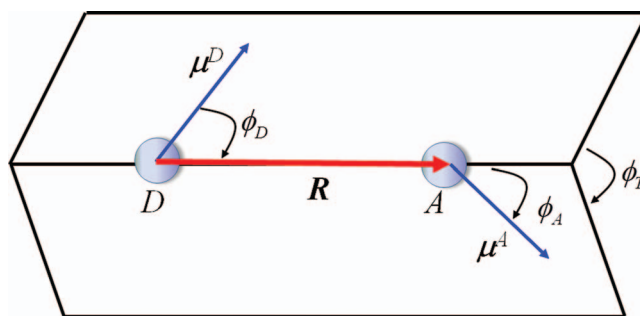

FIG. 2. The orientational factors, Eqs. (12) and (23), scale the coupling between an EET donor and acceptor. The parameters required to calculate the orientational factors are ϕ_D, the angle between the donor and the displacement vector, ϕ_A, the angle between the acceptor and the displacement vector, and ϕ_T, the angle between the two transition dipole moments.

physically distinct cases inviting consideration are $(\eta_1, \eta_3) = (\pm 1, \pm 1)$ and $(\eta_1, \eta_3) = (0, \pm 2)$.

The first case, where $(\eta_1, \eta_3) = (\pm 1, \pm 1)$, corresponds to situations when the transition dipole moments are parallel or antiparallel to each other, and both are perpendicular to the separation vector (see Fig. 1(b)). In this situation $\eta_1^2 = \eta_3^2 = \eta_1 \eta_3$, both short and long-range interactions are scaled by the same amount, leading to the coupling function

$$g(k, \mathbf{R}) = \frac{1}{|n|^4} \left\{ \frac{1}{k^6 R^6} + \frac{2n''}{k^5 R^5} + \frac{3n''^2 - n'^2}{k^4 R^4} \right.$$
$$\left. + \frac{2n''|n|^2}{k^3 R^3} + \frac{|n|^4}{k^2 R^2} \right\}. \quad (24)$$

Since for most frequencies of light, $n'^2 \gg 3n''^2$, the inverse 4th power term takes a negative sign, leading to a lower transfer rate at intermediate ranges except near resonances in the medium. Notably, this is different from the increased transfer rate that the same term produces, in the case of a randomly or isotropically oriented donor-acceptor pair.

The second case to be considered is when $(\eta_1, \eta_3) = (0, \pm 2)$. In this situation, the transition moment and displacement vector are collinear (i.e., any combination of parallel of antiparallel relative orientations – see Fig. 1(a)). The rate equation coupling term then becomes

$$g(k, \mathbf{R}) = \frac{1}{|n|^4} \left\{ \frac{4}{k^6 R^6} + \frac{8n''}{k^5 R^5} + \frac{4|n|^2}{k^4 R^4} \right\} \quad (25)$$

which contains no long-range coupling terms. This means that EET becomes negligible beyond the reduced wavelength ($\lambdabar = \lambda/2\pi$) of the energy transferred. However, at short ranges, the coupling is scaled by a factor of 4. Observe that the term in R^{-4} is specifically positive, further enhancing the rate of transfer. The lack of effective transfer in the far-zone corresponds to the fact that under the described conditions, the coupling would have to be essentially longitudinal, whereas photons propagating in this region would necessarily be almost entirely of transverse character.[5]

These results suggest that when designing an energy transfer system, such as an energy harvesting photosynthetic device, optimal configurations for fast transfer between nearby sites are those where the donor and acceptor transition dipole moments and the separation vector are collinear. Coupling may also be "switched off" between certain chromophores by arranging them such that the transition dipole moments are mutually orthogonal. This can, in effect, enable one to design molecular aggregate materials that are optimized to focus the energy transfer to specific points.

The case where the transition dipole moments of the donor and acceptor take random orientations is now considered. This is important, for example, when considering energy migration between disconnected donor and acceptor units, for example, in a liquid phase, where the medium between the donor and acceptor can be considered to be optically isotropic. The effect on the transfer rate may be calculated by taking a rotational average of the orientation factors as they appear in the coupling function: η_1^2, $\eta_1 \eta_2$, and η_3^2. The final form of the isotropic rate equation coupling terms is then

given by

$$\langle g(k, \mathbf{R}) \rangle = \frac{1}{|n|^4} \left\{ \frac{2}{3} \frac{1}{k^6 R^6} + \frac{4}{3} \frac{n''}{k^5 R^5} + \frac{2}{3} \frac{|n|^2}{k^4 R^4} + \frac{2}{9} \frac{|n|^4}{k^2 R^2} \right\}. \quad (26)$$

The derivation of this equation can be found in the Appendix.

Comparing Eq. (26) with (25) and (24), it can be seen that the rotational averaging, in general, dampens the coupling terms of the rate equation. This suggests that artificial energy transfer systems that possess chromophores that are randomly oriented with respect to one another will generally be less efficient than in materials where they are set. This is reflected in the numerical calculations, reported in subsequent sections.

B. Distance dependence

As observed earlier, in the originally derived form of the rate equation coupling, $g(k, \mathbf{R})$, for a donor and acceptor separated by vacuum, only three terms emerge. Namely, those proportional to the inverse-sixth, the inverse-fourth, and the inverse-square powers of the transfer distance, Eq. (11). The inverse sixth power term gives rise to the dominant contribution to the transfer rate in the short range limit ($k\mathbf{R} \ll 1$) while the inverse squared term gives rise to the long-range ($k\mathbf{R} \gg 1$) limit. The inverse fourth term is most significant at intermediate ranges ($k\mathbf{R} \sim 1$), i.e., when the distance between the chromophores is approximately equal to the reduced wavelength of the transferring photon (i.e., the order of 100 nm for UV/visible light). When EET occurs in the condensed phase, the existence of the imaginary part of the complex valued refractive index ensures that two additional terms emerge, namely, the inverse fifth and inverse cube terms in Eq. (17). The coupling contribution to the inverse ith term will be referred to as $g_i(\omega, \mathbf{R})$. Identifying the individual terms in Eq. (17), the explicit forms of $g_i(\omega, \mathbf{R})$ for $i = 2, 3, 4, 5, 6$, are as follows:

$$g_2(k, \mathbf{R}) = \eta_1^2 \frac{1}{k^2 R^2}, \quad (27)$$

$$g_3(k, \mathbf{R}) = \frac{1}{|n|^2} 2\eta_1 \eta_3 n'' \frac{1}{k^3 R^3}, \quad (28)$$

$$g_4(k, \mathbf{R}) = \frac{1}{|n|^4} \left[\eta_3^2 |n|^2 - 2\eta_1 \eta_3 (n'^2 - n''^2) \right] \frac{1}{k^4 R^4}, \quad (29)$$

$$g_5(k, \mathbf{R}) = \frac{1}{|n|^4} 2\eta_3^2 n'' \frac{1}{k^5 R^5}, \quad (30)$$

$$g_6(k, \mathbf{R}) = \frac{1}{|n|^4} \eta_3^2 \frac{1}{k^6 R^6}. \quad (31)$$

The range at which the odd-powered terms, $g_5(k, \mathbf{R})$ and $g_3(k, \mathbf{R})$ become important will now be established. The imaginary part of the refractive index is, of course, highly dependent on the wavelength of the light propagating through the medium. Generally speaking, n'' becomes large when the molecules comprising the condensed phase have an allowed electronic transition which is of similar magnitude to the transferred energy. This is clearly the case in molecular aggregates, such as thin film J-aggregates, where all molecules

are identical. It has been experimentally verified that organic thin film molecular aggregates mostly have refractive indices with large imaginary components at highly absorbing frequencies.[32] It is important to note the dispersion behavior of a condensed phase system, i.e., the imaginary part of the refractive index, can in general span several orders of magnitude for a particular medium. For example, in water the range is $\sim 10^{-9}$ to ~ 1.[33]

To examine the influence of the $g_5(k, R)$ and $g_3(k, R)$ rate contributions, the conditions for which they are equal to $g_6(k, R)$ will be considered. This will be the chromophore separation at which these terms significantly influence, and may start to dominate the EET process. Of particular interest is whether, for allowed values of the orientation factors and the refractive index, the magnitude of the couplings are in the regime $kR \ll 1$ is non-negligible.

The inverse fifth power term is considered first. Setting $g_6(k, R) = g_5(k, R)$, and solving for kR, gives the distance between the chromophores for which the two terms are equal

$$kR = \frac{1}{2n''}. \tag{32}$$

Consequently, for common values of n'' (i.e., $n'' \ll 1$), $g_5(k, R) = g_6(k, R)$ at $kR \gg 1$, and $g_5(k, R)$ is therefore negligible in most cases. However, the inclusion of this term may be important when considering the transfer of high-energy excitations over short distances in a highly absorbing medium or at near resonant frequencies. Fig. 3 shows the logarithmic plots of $g_6(k, R)$ and $g_5(k, R)$ against kR, with $\eta_3 = 1$, (a)

where $n'' = 10^{-5}$, (b) $n'' = 0.1$, (c) $n'' = 0.5$, and (d) $n'' = 1.0$, taking the real part of the refractive index as $n' = 1.9$.

For the case of the inverse cubic term, setting $g_3(k, R) = g_6(k, R)$, gives

$$kR = \left(\frac{\eta_3}{2\eta_1 |n|^2 n''}\right)^{\frac{1}{3}}. \tag{33}$$

Thus, as with $g_5(k, R)$, this term is negligible for $n'' \ll 1$. As the medium becomes more highly absorbing ($n'' \to 1$), the onset of significant contributions from this term depends on the orientation factors as well as the magnitude of the complex refractive index. The dependence on the orientation factor seriously complicates the analysis. However, it can be seen in cases where the two orientation terms are approximately equal (e.g., $\eta_1 \approx \eta_3 \approx \pm 1$, as is the case when the transition dipole moments are parallel or anti-parallel to each other and perpendicular to the separation vector), that $g_3(k, R) = g_6(k, R)$ in the range $kR < 1$. Consequently, the R^{-3} term is non-negligible in these situations.

For highly absorbing media where $n'' \gg 0$, there is a critical kR range where all of the different contributions in Eq. (17) play a role in the coupling. This could lead to major departures from Förster distance dependence, and may explain some of the behavior that has recently been seen in energy transfer studies in polymer-based nanostructured films.[20] Fig. 4 shows the contributions from the individual $g_i(k, R)$; $(i = 2, 3, 4, 5, 6)$, for a range of kR values where $\eta_1 = \eta_3 = 1$.

Figure 4 shows the distance dependence for (the absolute value of) the individual coupling terms, Eqs. (35)–(39), in the range $0.1 \leq kR \leq 2.0$. As can be anticipated, it is clear from
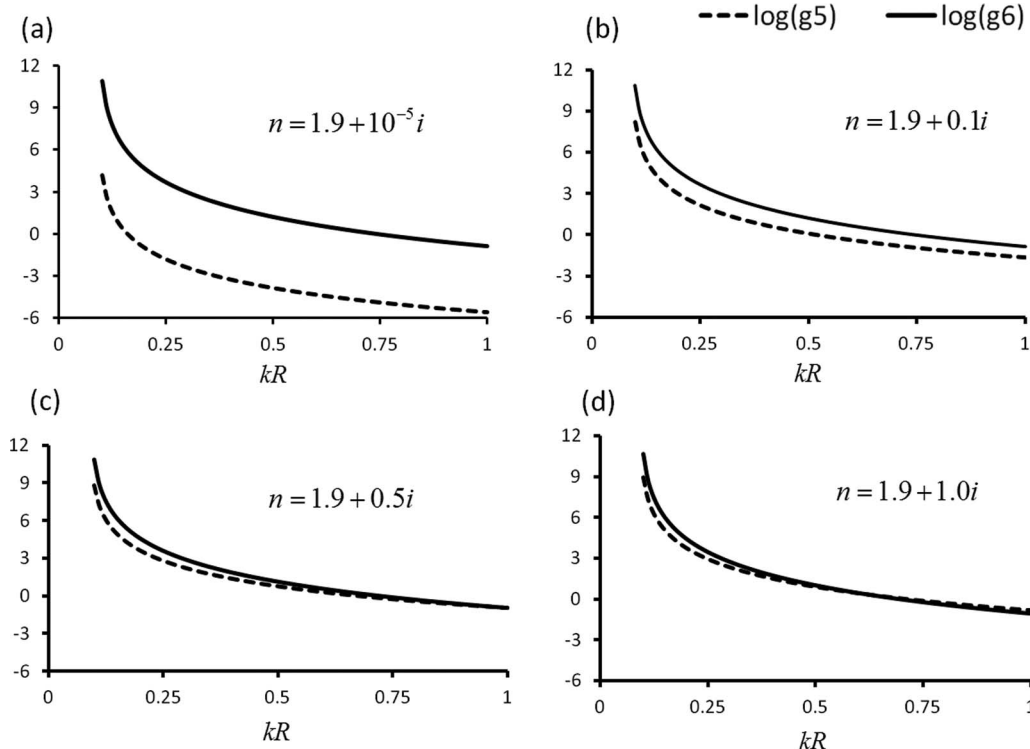

FIG. 3. The distance dependence of the R^{-5} (blue, dashed) and R^{-6} (red, solid) terms of the electronic coupling, Eqs. (30) and (31), respectively. Plot (a) shows that the R^{-6} term dominates for highly transparent media with a small imaginary component of the refractive index. However, as n'' become larger, the terms become of comparable magnitude, with the R^{-5} term dominating in highly absorbing media at large distances.
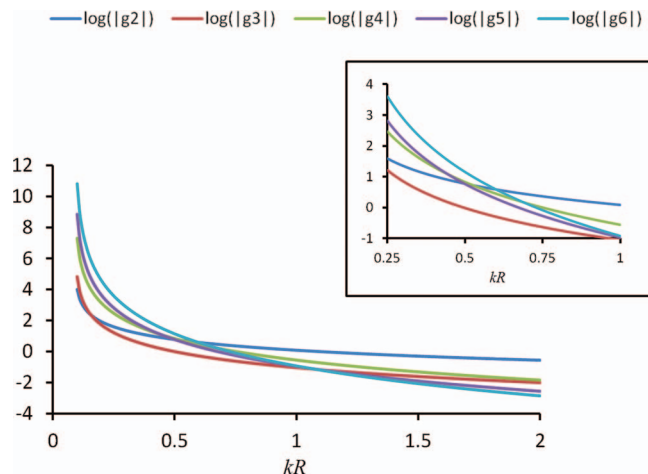
FIG. 4. Plots of the contributions from the individual rate equation coupling terms, $g_i(k, \mathbf{R})$, in Eq. (22) for an absorbing medium ($n = 1.9+0.5i$). The parameters are set as $\eta_1 = \eta_3 = \pm 1$. Note that for $g_4(k, \mathbf{R})$ the coupling magnitude is negative in this case, and consequently absolute values are shown.

FIG. 5. Schematic diagrams of 5×5 molecular grids. The molecules are assumed to be point particles separated by 2.5 nm. The arrows represent the transition dipole moments of the molecules. The first grid, (a), is the case of ordered transition dipole moments (TDM) where all TDMs lie in the direction of the x-axis. The second grid, (b), is the isotropic case, where all of the TDMs are randomly oriented in the xy-plane, but still centered on their respective grid points.

the main plot that the $g_6(k, \mathbf{R})$ term dominates at short distances, while the $g_2(k, \mathbf{R})$ term dominates at long distances. From the inset, one can see that within the range $0.5 \leq kR \leq 1.0$ the magnitude of the coupling components of the long range terms start to dominate over the short range ones. This is because it is in this range that the mediating photon begins to take on real (and hence transverse electric field) character, and there is a crossover from the nonradiative near-zone to the far-zone radiative coupling at approximately half the reduced wavelength.

C. Numerical calculations of the coupling terms for a molecular aggregate

In this section, the individual coupling terms are applied to a model system of a thin film molecular aggregate. The objective of this study is to obtain a realistic description for the electromagnetic coupling tensor and the rate equation coupling; these parameters are calculated for all molecules in the gird, with respect to the central molecule.

The numerical study involves setting up a two-dimensional grid of 41×41 generalized molecules, notionally 2.5 nm apart in both directions. The value of 2.5 nm was chosen to reflect approximate dimensions of typical florescent dye molecules that comprise organic molecular aggregates.[21] These conditions result in a square lattice of approximate dimensions 100 nm $\times$ 100 nm having a total of 1681 molecules. The coupling is calculated with respect to the molecule at the centre of the grid, labelled molecule 0 at point (0,0) in the xy-plane. The experimentally realistic value of $n = 1.9 + 0.5i$ is used for the complex refractive index.[32] The transition dipole moments and electronic excitation energy of the constituent molecules are taken to be 10.0 D and 3 eV, respectively, which are realistic values for many molecules comprising organic thin films.[21] For the transfer of energy at the blue end of the visible spectrum, the reduced wavelength is approximately 65 nm. Consequently, in the numerical simulations, the maximum value of kR is approximately 0.75, at the corners of the
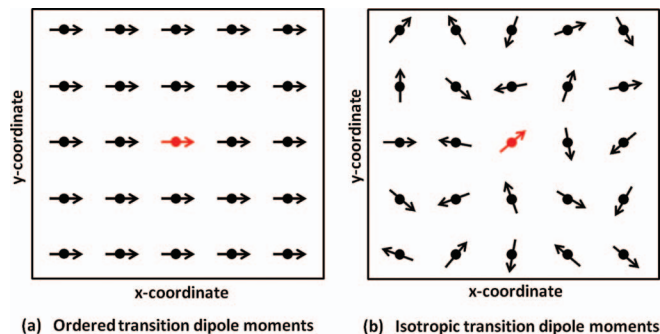
2D grids (see Figs. 6 and 7). Longer range effects ($kR > 1$) are considered in Sec. III D.

Two physically distinct situations are considered, namely, one where the transition dipole moments are ordered, all lying in the x-direction, and the other where they are randomly oriented. Fig. 5 presents a schematic depiction of the two cases considered. For clarity, only the central 25 molecules are displayed. The molecules are assumed to be point-like particles 2.5 nm apart from one another in both the x- and y-directions. The coupling is calculated with respect to the central (red) molecule. Fig. 5(a) corresponds to the case where the transition dipole moments are ordered, and Fig. 5(b) is the isotropic case.

The scalar coupling is calculated by contraction of the condensed phase electromagnetic coupling tensor with the transition dipole moments of the molecules in the grid

$$V_{n0}^{QED} = \langle n|T^{(2)}|0\rangle = \mu_{n_l}^{full}\theta_{lj}\mu_{0_j}^{full}. \quad (34)$$

Fig. 6 shows the magnitudes of the individual electromagnetic coupling terms for the 100 nm $\times$ 100 nm grid. Specifically, this figure displays the coupling between the centrally placed donor (denoted $|0\rangle$) and each of the other molecules on the grid ($|n\rangle$), for both ordered and randomly oriented transition dipole moments.

The full expression for the R^{-1}, R^{-2}, and R^{-3} contributions to the electromagnetic coupling of the nth molecule with the central molecule can be written in full as

$$V_{n0}^{R^{-i}}(k, \mathbf{R}) = \mu_{n_l}^{full}\theta_{lj}^{R^{-i}}\mu_{0_j}^{full}, \quad (35)$$

where

$$\theta_{lj}^{R^{-1}}(k, \hat{\mathbf{R}}) = -\frac{k^3 e^{iKR}}{4\pi\varepsilon_0}\left[(\delta_{lj} - \hat{R}_l\hat{R}_j)\frac{1}{kR}\right], \quad (36)$$

$$\theta_{lj}^{R^{-2}}(k, \mathbf{R}) = -\frac{k^3 e^{iKR}}{4\pi\varepsilon_0}\left[(\delta_{lj} - 3\hat{R}_l\hat{R}_j)\left(\frac{i}{k^2 R^2}\right)\right], \quad (37)$$

$$\theta_{lj}^{R^{-3}}(k, \hat{\mathbf{R}}) = \frac{k^3 e^{iKR}}{4\pi\varepsilon_0}\left[(\delta_{lj} - 3\hat{R}_l\hat{R}_j)\left(\frac{1}{k^3 R^3}\right)\right], \quad (38)$$
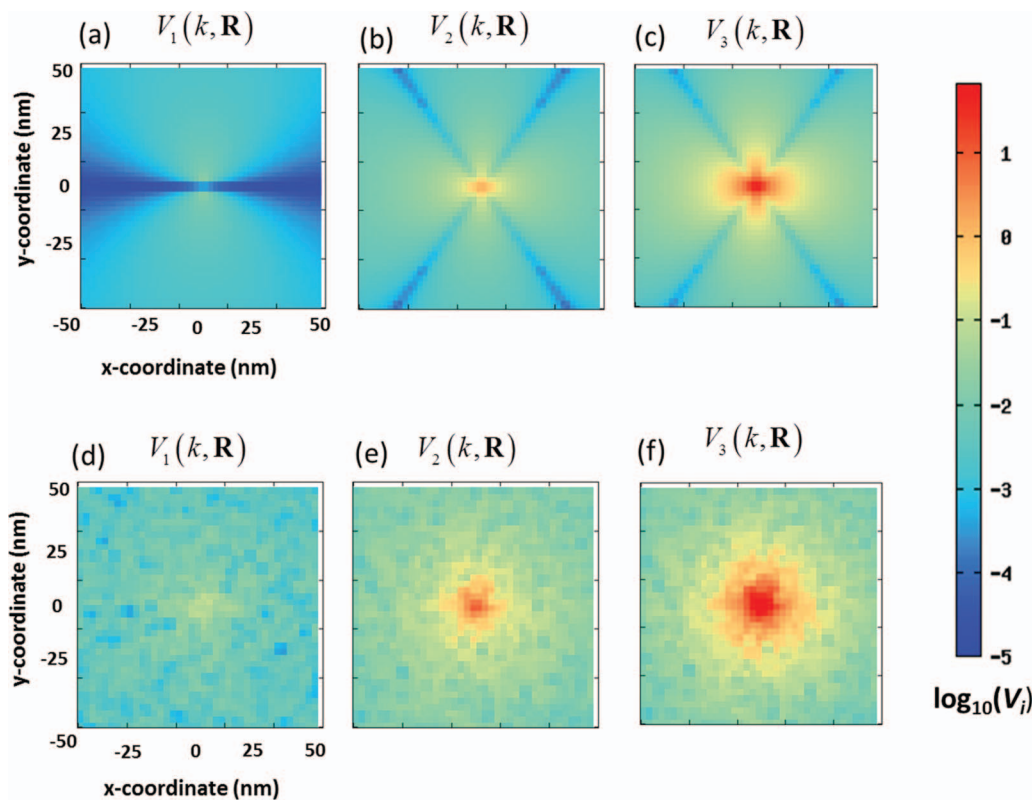
FIG. 6. (a)–(f) The R^{-1}, R^{-2}, and R^{-3} components of the electromagnetic coupling, $V(k, \mathbf{R})$, between the central molecule and the other molecules in the aggregate. All transition dipole moments are pointing in the x-direction for the upper panels, and are isotropic (randomly oriented in the plane) for the lower panels. Logarithmic plots are used for clarity.

and the full coupling is given by

$$V_{n0}^{QED} = \sum_{i=1}^{3} V_{n0}^{R^{-i}}. \tag{39}$$

The physical character of the electromagnetic coupling tensor can be understood most easily by considering Fig. 6, within the context of these equations. The upper part of Figs. 6(a)–6(c) shows the situation where the transition dipole moments are aligned in the x-direction, and the lower section of Figs. 6(d)–6(f) where the transition dipole moments are randomly oriented in the x,y-plane. It is important to note that the values of the electromagnetic tensor span several orders of magnitude. As one would expect, there is a region of very strong coupling about the central molecule for the R^{-3} term, with a significantly smaller region of strong coupling for the R^{-2} and no strong coupling for the R^{-1} contribution. The numerical calculations indicate that the radius of "strong" coupling is of the order of 10 nm for the R^{-3} term, and a few nanometers for the R^{-2}, based on the isotropic cases (Figs. 6(d)–6(f)).

It is interesting to consider the case in which the transition dipole moments are ordered. In this case, one can see that there is a very structured spatial dependence of the coupling. For $V_{n0}^{R^{-3}}$, there are four regions of strong coupling in the x (positive and negative) and y (positive and negative) directions. The strongest coupling is in the x-direction, where the transition dipole moment of molecules 0 and n are parallel to one another, and also to their mutual displacement vector. The result exemplifies an earlier comment that this strong

coupling occurs because, at short distances, the virtual photons that mediate the EET process have longitudinal character. Consequently, molecules with transition dipole moments parallel to one another and also parallel to the displacement vector are strongly coupled for $kR \ll 1$. However, it can be seen in Fig. 5(c) that there is also some strong coupling in the y-direction, because the virtual photons also have some transverse character at small distances. The shape of the strong coupling region for $V_{n0}^{R^{-2}}(k, \mathbf{R})$ is similar to that for $V_{n0}^{R^{-3}}(k, \mathbf{R})$ (as the orientational dependence $(\delta_{lj} - 3\hat{R}_l\hat{R}_j)$ is the same for both terms, Eqs. (37) and (38)), but falls away more rapidly. The spatial dependence of the long range coupling, $V_{n0}^{R^{-1}}(k, \mathbf{R})$ is particularly interesting as it is fundamentally different from the intermediate and short range coupling terms. The long range interactions are mediated exclusively by transverse virtual photons and consequently there is exactly zero coupling between the origin molecule and all other molecules lying along the x-axis (i.e., $y = 0$). The coupling then fans out in the positive and negative y-directions. The capacity to modify this feature by high-level laser scanning is, indeed, a feature that has attracted attention in connection with all-optical switching.[34,35]

Of particular interest is the very low magnitude coupling in the diagonal directions, for both $V_{n0}^{R^{-2}}(k, \mathbf{R})$ and $V_{n0}^{R^{-3}}(k, \mathbf{R})$. This arises, because in these regions the donor and acceptor transition dipole moments cannot be coupled strongly either by longitudinal or transverse electric fields.

A similar approach can be used for numerically analysing the individual terms that comprise the *rate equation coupling*
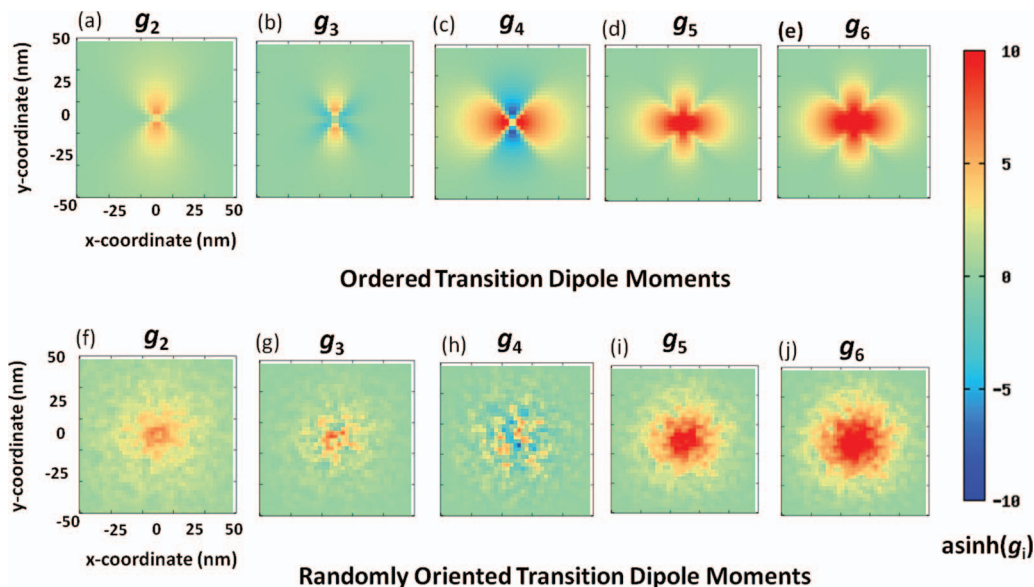
FIG. 7. (a)–(j) The R^{-2}, R^{-3}, R^{-4}, R^{-5}, R^{-6} components of the rate equation coupling, $g(k, \mathbf{R})$, between the central molecule and the other molecules in the aggregate. All transition dipole moments are pointing in the x-direction for the upper panels, and are isotropic (randomly oriented in the plane) for the lower panels. Asinh plots are used to emphasize weak coupling regions.

term for a condensed phase medium, Eq. (22). The coupling is considered in terms of the five fundamental components, Eqs. (35)–(39). The upper part of Figs. 7(a)–7(e) shows the individual coupling terms for an ordered set of transition dipole moments, all aligned along the x-axis. The lower part (Figs. 7(f)–7(j)) shows the couplings that arise when the orientation of the dipole moments are randomly distributed in the x,y-plane.

Inspection of Fig. 7 allows one to gain insight into how the spatial variation of the rate coupling, Eq. (22), is influenced by the individual contributing terms. It is important to note that $g_6(k, \mathbf{R})$, $g_4(k, \mathbf{R})$, and $g_2(k, \mathbf{R})$ in the rate equation coupling are analogous in their physical origins to $V_{n0}^{R^{-3}}(k, \mathbf{R})$, $V_{n0}^{R^{-2}}(k, \mathbf{R})$, and $V_{n0}^{R^{-1}}(k, \mathbf{R})$, respectively (although $g_4(k, \mathbf{R})$ does acquire some contributions from the interference of R^{-1} and R^{-3} terms). One can observe that the shapes of the region of strong coupling are quite similar. For example, $V_{n0}^{R^{-3}}(k, \mathbf{R})$ and $g_6(k, \mathbf{R})$ both have significant couplings along the x and y axes, with the coupling along the x-axis, most favourable.

It is interesting to consider the orientational dependence of $g_4(k, \mathbf{R})$, in the case of condensed phase EET. There are two different contributions that this term makes. It is additive with respect to the total coupling, Eq. (17), in the x-direction, when the transition dipole moments are parallel to the displacement vector, and subtracts from the total coupling in the y direction, when the transition dipole moments are perpendicular to the displacement vector. These results are clearly consistent with Eqs. (24) and (25), which give the analytical expressions when the transition dipole moments are perpendicular and parallel to the displacement vector, respectively.

In the case of the rate equation couplings, the far-zone terms, $g_2(k, \mathbf{R})$ and $g_3(k, \mathbf{R})$ can be seen to have shorter ranges of influence than the $V_{n0}^{R^{-1}}(k, \mathbf{R})$ term in the electromagnetic tensor coupling, due to the fact that squaring the weak interactions significantly dampens them. The profile is however similar, as expected.

D. Numerical simulations: Short-range hopping verses direct long-range transfer

In order to quantify the extent to which long range electronic coupling terms may be involved in the electronic energy transfer process in molecular aggregates, one must compare the population dynamics derived from Förster theory with that derived from the QED coupling terms, Eq. (17). More precisely, the question we seek to ask is: Under what circumstances does short range incoherent hopping out-compete long range coherent transfer? There are at least two different approaches that could be undertaken to analyse this. The first is a quantum dynamics approach where the time dependent wavefunction (or density matrix) is propagated directly using the electronic Hamiltonian, as is done in numerous past studies.[4,6,36–40] The other approach employs the PME, where the rate constants are used to describe the population transfer between sites.[6,41–44] It is important to point out that while the first approach explicitly includes quantum coherent effects into the dynamics, the PME approach describes incoherent transport, with quantum effects (i.e., interference terms) being included implicitly through the rate constants.

In this study, long range transfer is of particular importance, and hence it is computationally more tractable to model the time dependence of exciton diffusion on a 1D lattice, rather than a 2D grid. As outlined below, by altering the orientation of the TDMs with respect to 1D lattice, insight into the dynamics of EET occurring in different directions on the 2D grids (Fig. 8) can be gained. In the simulations, electronic energy transfer occurs from the initially excited molecule in the center of the 1D lattice. The exciton diffusion process is modelled kinetically by evaluating PMEs,

$$\frac{d}{dt} P_\mu(t) = \sum_{\mu \neq \nu}^{N} [W_{\mu \leftarrow \nu} P_\nu(t) - W_{\nu \leftarrow \mu} P_\mu(t)]. \qquad (40)$$

This set of equations describes the dynamics of the population on site μ with reference to all other sites in the molecular aggregate. Here, P_μ is the electronic population on the μth site and $W_{\mu \leftarrow \nu}$ is the rate constant for the transfer of population from site ν to μ.

In this study we seek, specifically, to compare the dynamics obtained when only Förster coupling is used, i.e., the R^{-6} term only, Eq. (31) to calculate the rate constants, and when the full QED coupling, Eq. (17), is employed to calculate the rate constants. Direct calculation of the rate constants using Eq. (16) requires the knowledge of some empirical parameters such as the radiative lifetime of the donor and spectral overlap between the absorption cross-section of the acceptor and the emission spectrum of the donor. These parameters have been chosen in a phenomenologically consistent way. A reasonable estimate for the radiative lifetime, τ_D, of chromophore that may be found in a molecular aggregate, such as a J-aggregate, would be about 1 ps.[45] Estimating the spectral overlap parameter, on the other hand, is more complicated. It turns out to be more convenient to recast the rate Eq. (16) in terms of the Förster radius. The rate equation for short range Förster coupling can be rewritten as

$$W_{DA}^{(R^{-6})} = \frac{9c^4\eta_3^2}{8\pi\tau_D R^6} \int_0^\infty F_D(\omega)\sigma_A(\omega)|n|^{-4}\omega^{-4}e^{-2n''\omega R/c}$$

$$= \frac{1}{\tau_D}\left(\frac{R_0}{R}\right)^6, \qquad (41)$$

where all terms, except the radiative lifetime and the distance between the chromophores become subsumed into the R_0^6 term. Förster radii are documented for many chromophores and form the basis of the *spectroscopic ruler*.[45,46] It is important to realize that when the rate is written in terms of the Förster radius the orientational factor, η_2^3, is replaced by its rotationally averaged value, of $\eta_2^3 = 2/3$. Consequently, in order to incorporate orientational effects into the simulations, we must factor this out the expression, Eq. (41). The rate equation for Förster coupling is now written as

$$W_{DA}^{(R^{-6})} = \left(\frac{3}{2}\right)^{\frac{1}{6}}\frac{\eta_3^2}{\tau_D}\left(\frac{R_0}{R}\right)^6. \qquad (42)$$

In order to employ Förster radii for the calculation of the other contributions to the rate equation, two assumptions must be made. Namely, that the frequencies, ω, of spectral overlap region are significantly smaller than the excitation frequency and that the refractive index is constant over the spectral overlap region. Once we have made these reasonable assumptions, we may rewrite the individual contributions to the rate constant in terms of the Förster radii,

$$W_{DA}^{(R^{-5})} = \left(\frac{3}{2}\right)^{\frac{1}{6}}\frac{k}{\tau_D}\left[\eta_3^2 2n''\right]\left(\frac{R_0^6}{R^5}\right), \qquad (43)$$

$$W_{DA}^{(R^{-4})} = \left(\frac{3}{2}\right)^{\frac{1}{6}}\frac{k^2}{\tau_D}\left[\eta_3^2|n|^2 - 2\eta_1\eta_3(n'^2 - n''^2)\right]\left(\frac{R_0^6}{R^4}\right), \qquad (44)$$

$$W_{DA}^{(R^{-3})} = \left(\frac{3}{2}\right)^{\frac{1}{6}}\frac{k^3}{\tau_D}\left[2\eta_1\eta_3 n''|n|^2\right]\left(\frac{R_0^6}{R^3}\right), \qquad (45)$$

$$W_{DA}^{(R^{-2})} = \left(\frac{3}{2}\right)^{\frac{1}{6}}\frac{k^4}{\tau_D}\left[\eta_1^2|n|^4\right]\left(\frac{R_0^6}{R^2}\right), \qquad (46)$$

$$W_{DA} = W_{DA}^{(R^{-6})} + W_{DA}^{(R^{-5})} + W_{DA}^{(R^{-4})} + W_{DA}^{(R^{-3})} + W_{DA}^{(R^{-2})}. \qquad (47)$$

Equations (42)–(47) will be used as the rate constants to evolve the population dynamics, by numerical integration of Eq. (40). The purpose of the PME simulations, is to determine the whether direct far-zone EET will outcompete short-range incoherent hopping in molecular aggregates. We consider energy migration along a linear chain of molecules, as has been done in previous studies.[47,48] Three different kinds of 1D lattice are considered with the TDMs arranged as shown in Figure 8. The Förster radius used in the simulations is 3.8 nm, in-line with that for a variety of dye molecules.[45] As with the 2D grid calculations, the transition dipole moments and electronic excitation energy of the constituent molecules are 10.0 D and 3 eV, respectively.

The chain comprises 201 molecules, each separated by 2.5, 5.0, or 7.5 nm. This means that the distance within which EET can occur within the simulations far exceeds the reduced wavelength of the mediating virtual photon, in all cases. The exciton population is initially localized on the central molecule at time zero. Figs. 9–11 display the results of the simulations. For each of the figures, panels (a), (b), and (c) correspond to linear chains with transition dipole moments parallel, perpendicular, and at a 45° angle to the displacement vector, respectively. Fig. 9 corresponds to a 1D lattice where the individual molecules are 2.5 nm apart, while Figs. 10 and 11 correspond to lattices with molecules separated by 5.0 and 7.5 nm, respectively. The black lines correspond to the population dynamics when the full coupling is calculated from Eq. (47). The dashed blue line corresponds to the dynamics obtained using the Förster coupling only, Eq. (41). The dynamics was also analysed for the individual terms, Eqs. (43)–(46). All plots show the population decay from the initially excited central molecular center. Note that for clarity in observing differences between Förster and full QED dynamics, the time scales differ for different lattices.
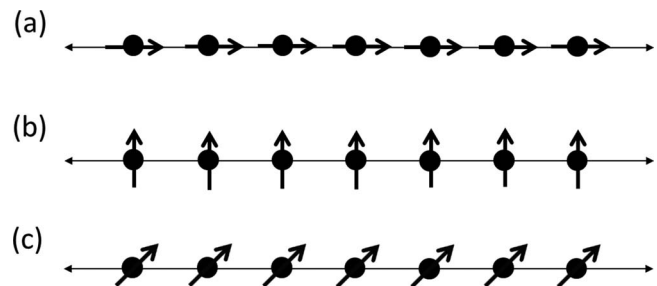

FIG. 8. Schematic diagrams for the orientation of the transition dipole moments of the one-dimensional lattice of molecules. (a) The top lattice shows that the TDMs are parallel to the displacement vector (i.e., lying along the x-axis). (b) In the case of the second lattice, the TDMs are perpendicular to the displacement vector (i.e., in the y-direction). (c) The third case is where they are at a 45° angle.
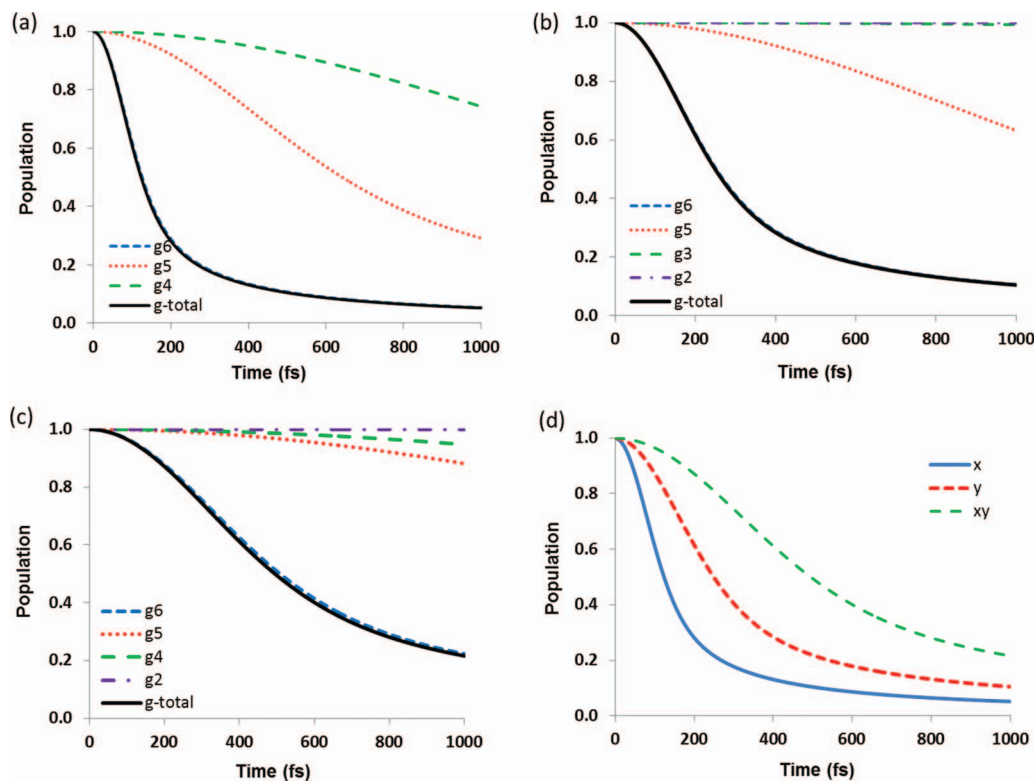
FIG. 9. Population of the central (initially fully populated) chromophore as a function of time for a one-dimensional lattice, with 2.5 nm between molecular centers. (a) TDMs pointing in the x-direction, (b) TDMs pointing in the y-direction, (c) TDMs pointing at $y = x$. In legend, g6 corresponds to dynamics of $W_{DA}^{(R^{-6})}$, etc. Panel (d) shows the population decay for each of the TDM orientations.
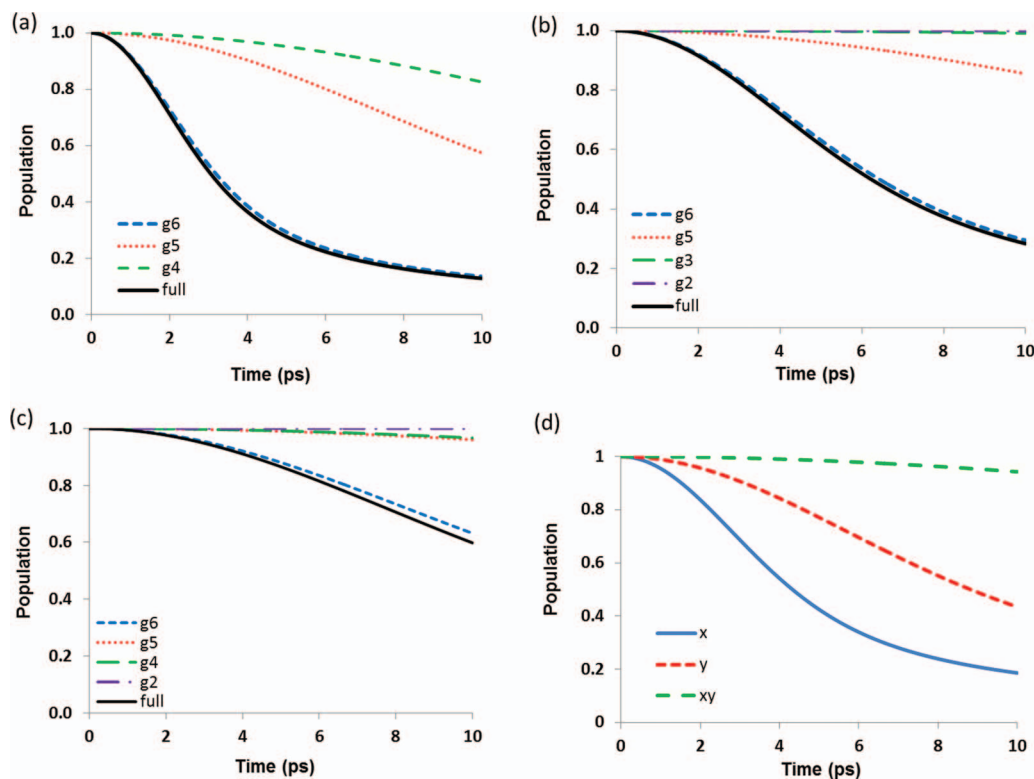

FIG. 10. (a)–(d) As for Figure 9, but with a distance of 5.0 nm between molecular centers on the one-dimensional lattice.
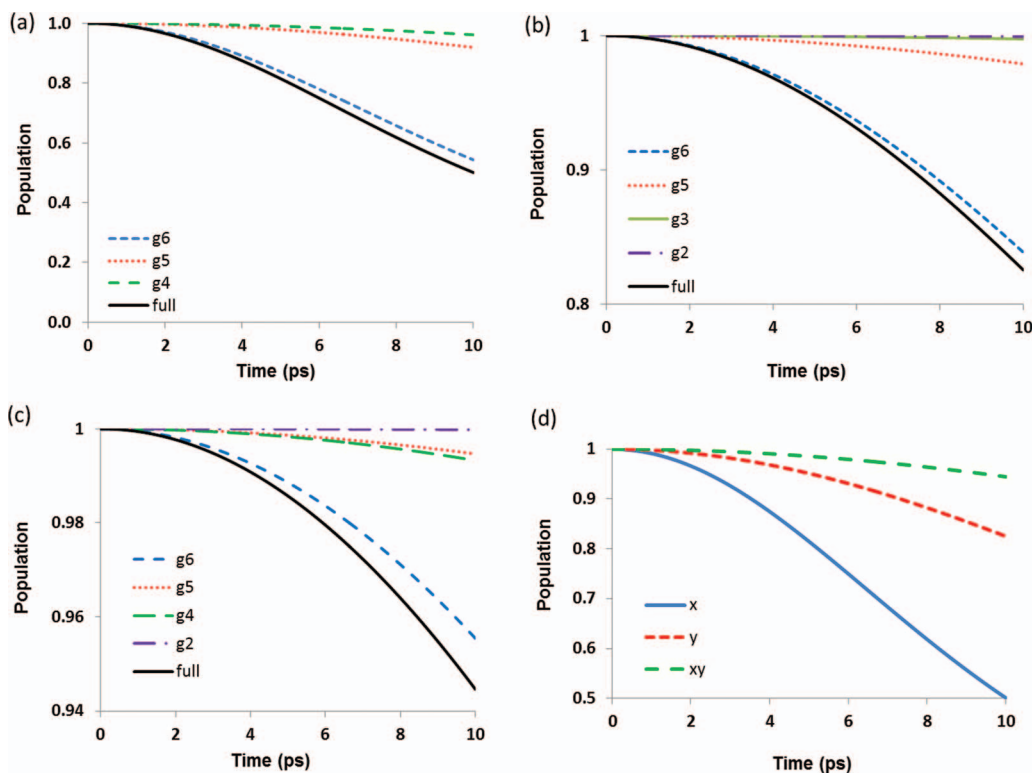
FIG. 11. (a)–(d) As for Figure 9, but with a distance of 7.5 nm between the molecular centers on the one-dimensional lattice.

From these results, it can be seen that short range Förster coupling generally agrees very well with the full QED derived coupling for molecular aggregates, irrespective of the orientation of the transition dipole moments. This is especially the case for aggregates where the molecular species are close to one another, as is the case in Fig. 9, where the molecules are separated by 2.5 nm. This indicates that Förster coupling should, in general, be valid for molecular aggregates, such as H- and J-aggregates, even when exciton diffusion occurs over long distances. However, as the distance between the individual molecules increases, the intermediate and far-zone terms start to play a role in the dynamics. Therefore, consideration of these terms could become important for designing mesoscopic energy transporting and harvesting materials, such as quantum dot arrays, where the distance between individual quantum dot centers can exceed 5 nm.[49–52]

Panel (d) in Figs. 9–11 compare the population dynamics, based on the rate constant derived from full QED coupling Eq. (47), for the different orientations of the transition dipole moments. These figures are very revealing in displaying the importance of the relative orientations of the transition dipole moments within molecular aggregates. It can be clearly seen that the optimal configuration for exciton transport is that the transition dipole moments be parallel to one another, and parallel to the displacement vector. Transport efficiency is also quite good when the transition dipole moments are perpendicular to the displacement vector. However, the intermediate case, where they are at a 45° angle to the displacement vector results in poor transport. This reflects what we have already seen in the analysis of the coupling terms in Figs. 6 and 7, where the strongest coupling for the R^{-6} term is exactly along

the x- and y-axes, while the diagonal, y = x, shows very poor coupling.

Finally, EET dynamics based on the PME for the simple case of a single exciton donor and acceptor is considered. Specifically, we are interested in determining the extent to which the intermediate and far-zone terms affect the dynamics between a single donor and a single acceptor, as a function of distance. This is important from the point of view of the *spectroscopic ruler*,[45] a technique that employs FRET (Förster resonance energy transfer) to establish distance between molecular species, by measuring the transport rate of the exciton and assuming that the rate constant has a R^{-6} distance dependence between chromophores. Although this has shown, time and time again, to be a powerful and important technique utilised in many areas of material and biological research, it has come under significant criticism because of its departure from the R^{-6} trend.[53–60]

Here, the PME are again employed, but this time for a two site system. If we assume that the exciton is instantaneously trapped on the acceptor, the PMEs can be rewritten as

$$P_D = \exp(-k_{A \leftarrow D} t), \qquad (48)$$

$$P_A = [1 - \exp(-k_{D \leftarrow A} t)], \qquad (49)$$

where P_D and P_A are the populations on the donor and acceptor, respectively.

Figs. 12 and 13 show the time dependence of the donor population as a function of time, for two different orientations of the transition dipole moments. The panels (a)–(d)
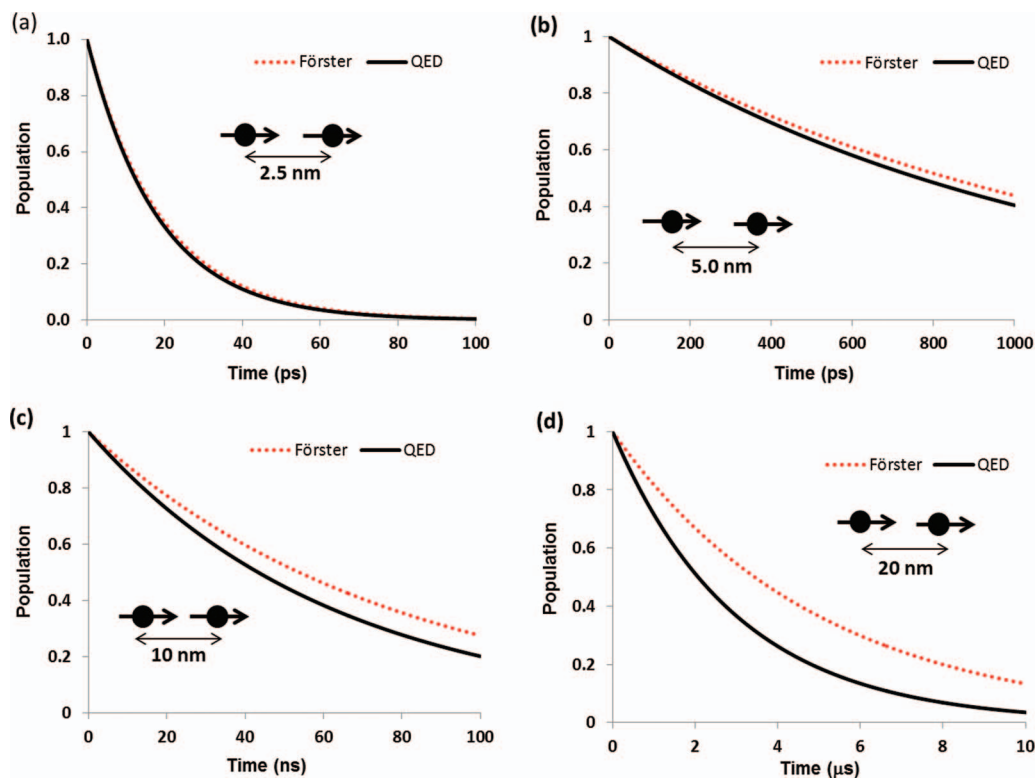
FIG. 12. (a)–(d) Population decay for an exciton donor acceptor pair with TDMs parallel to the displacement vector. The separation distances are shown in the figure.
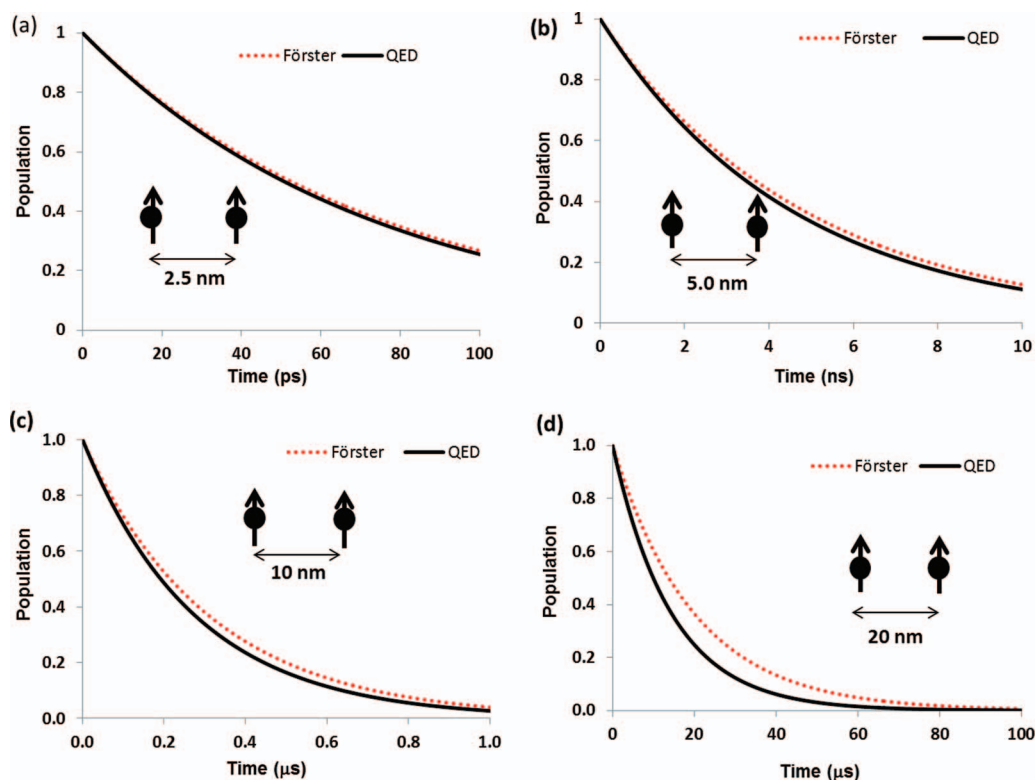

FIG. 13. (a)–(d) Population decay for an exciton donor acceptor pair with TDMs perpendicular to the displacement vector. The separation distances are shown in the figure.

correspond to separations between the two chromophores of 2.5, 5.0, 10.0, and 20.0 nm. It can be clearly seen that while the Förster coupling correctly describes the dynamics for chromophore separations that are less than 10 nm, there is an obvious discrepancy for chromophore separations in excess of this distance. It is interesting to note that a R^{-4} dependence on rates of EET has been seen in numerous studies, where the chromophores are separated by distances larger than 10 nm.[54,56,58]

IV. CONCLUSIONS

The focus of this study on EET has been to investigate, analytically and numerically, the spatial dependence of the electromagnetic coupling tensor, Eq. (15), and the rate equation coupling, Eq. (17). These two parameters, one quadratically related to the other and derived from the theory of quantum electrodynamics, are fundamental parameters for correctly describing long range EET within a condensed phase environment. The former is analogous to off-diagonal coupling terms that appear in the usual site basis EET Hamiltonian, while the latter is the fundamental parameter appearing in the Fermi Golden Rule rate equation. Further, Pauli Master Equations have been applied to model the dynamics of EET in one-dimensional lattices, as well as donor-acceptor pairs.

The results have demonstrated the intricate interplay of distance and orientational factors determining the efficiency of energy transfer. Although Förster Theory is very well suited to many situations, often providing qualitatively and quantitatively accurate description of the energy transfer process, the distance dependence for EET coupling is more complicated than traditional Förster Theory predicts. Further, its influence is significantly modified by the orientational dependence. The origin of these complications is deeply rooted in the nature of the virtual photon, or polariton, mediating the transfer process.

These factors invite reconsideration of the widely applied assumptions in the analysis of energy transfer in molecular aggregates, particularly since it emerges that the transfer efficiency might be significantly higher than standard theory suggests – especially when the host medium for the donor and acceptor chromophores has a significant imaginary term in its refractive index. In particular, the population dynamics simulations indicate that consideration of all coupling may be essential for describing spectroscopic ruler experiments which, on numerous occasions, have been shown to violate the assumed R^{-6} dependence of Förster Theory.

Further, when designing artificial photosynthetic systems, it may be beneficial to make use of optimal orientation of the transition dipole moments of the chromophores comprising the medium. A recent review has remarked that we can take "lessons from nature" when designing supramolecular structures for solar energy harvesting, points towards several important physical principles, including quantum coherence and photoprotection.[61] It may also be important to take into consideration the nature of individual mediating photons and polaritons when investigating EET in these types of systems.

APPENDIX: A MATHEMATICAL PROOF OF EQ. (26)

Here, the derivation of Eq. (26) is given. The orientational factors are expressed in full as

$$\eta_1^2 = (\hat{\boldsymbol{\mu}}_a \cdot \hat{\boldsymbol{\mu}}_d) + (\hat{\mathbf{R}} \cdot \hat{\boldsymbol{\mu}}_a)^2 (\hat{\mathbf{R}} \cdot \hat{\boldsymbol{\mu}}_d)^2$$
$$- 2(\hat{\boldsymbol{\mu}}_a \cdot \hat{\boldsymbol{\mu}}_d)(\hat{\mathbf{R}} \cdot \hat{\boldsymbol{\mu}}_a)(\hat{\mathbf{R}} \cdot \hat{\boldsymbol{\mu}}_d), \tag{A1}$$

$$\eta_1 \eta_3 = (\hat{\boldsymbol{\mu}}_a \cdot \hat{\boldsymbol{\mu}}_d) + 3(\hat{\mathbf{R}} \cdot \hat{\boldsymbol{\mu}}_a)^2 (\hat{\mathbf{R}} \cdot \hat{\boldsymbol{\mu}}_d)^2$$
$$- 6(\hat{\boldsymbol{\mu}}_a \cdot \hat{\boldsymbol{\mu}}_d)(\hat{\mathbf{R}} \cdot \hat{\boldsymbol{\mu}}_a)(\hat{\mathbf{R}} \cdot \hat{\boldsymbol{\mu}}_d), \tag{A2}$$

$$\eta_3^2 = (\hat{\boldsymbol{\mu}}_a \cdot \hat{\boldsymbol{\mu}}_d) + 9(\hat{\mathbf{R}} \cdot \hat{\boldsymbol{\mu}}_a)^2 (\hat{\mathbf{R}} \cdot \hat{\boldsymbol{\mu}}_d)^2$$
$$- 6(\hat{\boldsymbol{\mu}}_a \cdot \hat{\boldsymbol{\mu}}_d)(\hat{\mathbf{R}} \cdot \hat{\boldsymbol{\mu}}_a)(\hat{\mathbf{R}} \cdot \hat{\boldsymbol{\mu}}_d). \tag{A3}$$

To secure a result applicable to an entirely randomly oriented system, the donor and acceptor transition moments must be rotationally averaged with respect to each other, and both of them with respect to their mutual displacement vector. As rotational averaging is a linear operation, the values of η_1^2, $\eta_1\eta_2$, and η_3^2 follow from the averages of $(\hat{\boldsymbol{\mu}}_a \cdot \hat{\boldsymbol{\mu}}_d)^2$, $(\hat{\mathbf{R}} \cdot \hat{\boldsymbol{\mu}}_a)^2 (\hat{\mathbf{R}} \cdot \hat{\boldsymbol{\mu}}_d)^2$, and $(\hat{\boldsymbol{\mu}}_a \cdot \hat{\boldsymbol{\mu}}_d)(\hat{\mathbf{R}} \cdot \hat{\boldsymbol{\mu}}_a)(\hat{\mathbf{R}} \cdot \hat{\boldsymbol{\mu}}_d)$. Denoting components referring to the axis of a laboratory-fixed frame by i and j, the term $(\hat{\boldsymbol{\mu}}_a \cdot \hat{\boldsymbol{\mu}}_d)^2$ may be rewritten as

$$(\hat{\boldsymbol{\mu}}_a \cdot \hat{\boldsymbol{\mu}}_d)^2 = \mu_i^a \mu_i^d \mu_j^a \mu_j^d, \tag{A4}$$

where summation over repeated indices is assumed. Choosing a molecular basis that is attached to the donor chromophore (whose axes are labelled by λ and ν), a component of the donor transition dipole moment in the laboratory-fixed frame may be written as a sum of its components in the donor-fixed frame, each multiplied by the cosine of the angle between the laboratory axis and the donor-fixed axis or,

$$\langle \mu_i^a \mu_i^d \mu_j^a \mu_j^d \rangle = \langle \mu_i^a (l_{i\lambda}\mu_\lambda^d) \mu_j^a (l_{j\nu}\mu_\nu^d) \rangle = \mu_i^a \mu_\lambda^d \mu_j^a \mu_\nu^d \langle l_{i\lambda} l_{j\mu} \rangle, \tag{A5}$$

where $l_{i\lambda}$ denotes the cosine of the angle between axes represented by i and λ, and the angular brackets denote the rotational average. Since $\langle l_{i\lambda} l_{j\nu} \rangle = \frac{1}{3}\delta_{ij}\delta_{\lambda\nu}$, it follows that

$$\langle (\hat{\boldsymbol{\mu}}_a \cdot \hat{\boldsymbol{\mu}}_d)^2 \rangle = \mu_i^a \mu_\lambda^d \mu_j^a \mu_\nu^d \left(\frac{1}{3}\delta_{ij}\delta_{\lambda\nu} \right)$$

$$= \frac{1}{3}\mu_i^a \mu_\lambda^d \mu_j^a \mu_\nu^d$$

$$= \frac{1}{3}|\hat{\boldsymbol{\mu}}_a|^2 |\hat{\boldsymbol{\mu}}_b|^2$$

$$= \frac{1}{3}.$$

Following a similar procedure for $(\hat{\mathbf{R}} \cdot \hat{\boldsymbol{\mu}}_a)^2 (\hat{\mathbf{R}} \cdot \hat{\boldsymbol{\mu}}_d)^2$ and $(\hat{\boldsymbol{\mu}}_a \cdot \hat{\boldsymbol{\mu}}_d)(\hat{\mathbf{R}} \cdot \hat{\boldsymbol{\mu}}_a)(\hat{\mathbf{R}} \cdot \hat{\boldsymbol{\mu}}_d)$ allows one to derive

$$\langle (\hat{\mathbf{R}} \cdot \hat{\boldsymbol{\mu}}_a)^2 (\hat{\mathbf{R}} \cdot \hat{\boldsymbol{\mu}}_d)^2 \rangle = \frac{1}{9}$$

and

$$\langle (\hat{\boldsymbol{\mu}}_a \cdot \hat{\boldsymbol{\mu}}_d)(\hat{\mathbf{R}} \cdot \hat{\boldsymbol{\mu}}_a)(\hat{\mathbf{R}} \cdot \hat{\boldsymbol{\mu}}_d) \rangle = \frac{1}{9}.$$

Combining all of these expressions allows one to determine rotationally averaged values for the orientational factors, namely,

$$\langle \eta_1^2 \rangle = \frac{1}{3} + \frac{1}{9} - \frac{2}{9} = \frac{1}{9},$$

$$\langle \eta_1 \eta_3 \rangle = \frac{1}{3} + \frac{1}{3} - \frac{2}{3} = 0,$$

$$\langle \eta_3^2 \rangle = \frac{1}{3} + 1 - \frac{2}{3} = \frac{2}{3}.$$

Consequently, the rotationally averaged coupling function, Eq. (26) is given by

$$\langle g(k, \mathbf{R}) \rangle = \frac{1}{|n|^4} \left\{ \frac{2}{3} \frac{1}{k^6 R^6} + \frac{4}{3} \frac{n''}{k^5 R^5} + \frac{2}{3} \frac{|n|^2}{k^4 R^4} + \frac{2}{9} \frac{|n|^4}{k^2 R^2} \right\}.$$

[1] V. M. Agranovich and M. D. Galanin, *Electronic Excitation Energy Transfer in Condensed Matter* (Elsevier, Amsterdam, The Netherlands, 1982).

[2] B. Wieb Van derMeer, G. Coker III, and S.-Y. Chen, *Resonance Energy Transfer: Theory and Data* (VCH, New York, 1994).

[3] D. L. Andrews and A. A. Demidov, *Resonance Energy Transfer* (Wiley, New York, 1999).

[4] V. May and O. Kühn, *Charge and Energy Transfer in Molecular Systems* (Wiley-VCH, New York, 2011).

[5] D. L. Andrews and D. S. Bradshaw, "Virtual photons, dipole fields and energy transfer: A quantum electrodynamical approach," Eur. J. Phys. **25**, 845–858 (2004).

[6] See, for example, S. Mukamel, *Principles of Nonlinear Optical Spectroscopy* (Oxford University Press, Oxford, 1995).

[7] G. Grynberg, A. Aspect, and C. Fabre, *Introduction to Quantum Optics: From the Semi-classical Approach to the Quantized Limit* (Cambridge University Press, Cambridge, 2010).

[8] T. Förster, "Zwischenmolekulare Energiewanderung und Fluoreszenz," Ann. Phys. **437**, 55–75 (1948).

[9] S. F. Kilin and I. M. Rozman, "Effect of reabsorption on the fluorescence lifetimes of organic substances," Opt. Spectrosc. **6**, 40–44 (1959).

[10] J. S. Avery, "Resonance energy transfer and spontaneous photon emission," Proc. Phys. Soc. **88**, 1–8 (1966).

[11] D. L. Andrews and B. S. Sherborne, "Resonant excitation transfer: A quantum electrodynamical study," J. Chem. Phys. **86**, 4011–4017 (1987).

[12] D. L. Andrews, "A unified theory of radiative and radiationless molecular energy transfer," Chem. Phys. **135**, 195–201 (1989).

[13] G. J. Daniels, R. D. Jenkins, D. S. Bradshaw, and D. L. Andrews, "Resonance energy transfer: The unified theory revisited," J. Chem. Phys. **119**, 2264–2274 (2003).

[14] G. Juzeliūnas and D. L. Andrews, "Quantum electrodynamics of resonance energy transfer," Adv. Chem. Phys. **112**, 357–410 (2000).

[15] K. Bernhardt and H.-W. Trissl, "Theories for kinetics and yields of fluorescence and photochemistry: how, if at all, can different models of antenna organization be distinguished experimentally?," Biochim. Biophys. Acta **1409**, 125–142 (1999).

[16] J. Strümpfer, M. Şener, and K. Schulten, "How quantum coherence assists photosynthetic light harvesting," J. Phys. Chem. Lett. **3**, 536–542 (2012).

[17] Q. Zhang, T. Atay, J. R. Tischler, M. S. Bradley, V. Bulovic, and A. V. Nurmikko, "Highly efficient resonant coupling of optical excitations in hybrid organic/inorganic semiconductor nanostructures," Nat. Nanotechnol. **2**, 555–559 (2007).

[18] J. E. Halpert, J. R. Tischler, G. Nair, B. J. Walker, W. H. Liu, V. Bulovic, and M. G. Bawendi, "Electrostatic formation of quantum dot/J-aggregate FRET pairs in solution," J. Phys. Chem. C **113**, 9986–9992 (2009).

[19] Y. Shirasaki, P. O. Anikeeva, J. R. Tischler, M. S. Bradley, and V. Bulovic, "Efficient Forster energy transfer from phosphorescent organic molecules to J-aggregate thin films," Chem. Phys. Lett. **485**, 243–246 (2010).

[20] L. A. Cury, K. N. Bourdakos, D. Dai, F. B. Dias, and A. P. Monkman, "Long range energy transfer in conjugated polymer sequential bilayers," J. Chem. Phys. **134**, 104903 (2011).

[21] S. Valleau, S. K. Saikin, M.-H. Yung, and A. A. Guzik, "Exciton transport in thin-film cyanine dye J-aggregates," J. Chem. Phys. **137**, 034109 (2012).

[22] G. de Miguel, M. Ziolek, M. Zitnan, J. A. Organero, S. S. Pandey, S. Hayase, and A. Douhal, "Photophysics of H- and J-aggregates of indole-based squaraines in solid state," J. Phys. Chem. C **116**, 9379–9389 (2012).

[23] D. Melnika, D. Savateeva, V. Lesnyak, N. Gaponik, Y. N. Fernandez, M. I. Vasilevskiy, M. F. Costa, K. E. Mochalov, V. Oleinikov, and Y. P. Rakovich, "Resonance energy transfer in self-organized organic/inorganic dendrite structures," Nanoscale **5**, 9317–9323 (2013).

[24] A. Zangwill, *Modern Electrodynamics* (Cambridge University Press, Cambridge, 2013), p. 22.

[25] D. P. Craig and T. Thirunamachandran, *Molecular Quantum Dynamics* (Academic Press, London, 1984).

[26] J. A. Heras, "A short proof that the Coulomb-gauge potentials yield the retarded fields," Eur. J. Phys. **32**, 213–216 (2011).

[27] S. M. Barnett, R. P. Cameron, and A. M. Yao, "Duplex symmetry and its relation to the conservation of optical helicity," Phys. Rev. A **86**, 013845 (2012).

[28] E. M. Rice, D. S. Bradshaw, K. Saadi, and D. L. Andrews, "Identifying the development in phase and amplitude of dipole and multipole radiation," Eur. J. Phys. **33**, 345–358 (2012).

[29] A. Salam, "Mediation of resonance energy transfer by a third molecule," J. Chem. Phys. **136**, 014509 (2012).

[30] D. L. Andrews and J. S. Ford, "Resonance energy transfer: Influence of neighboring matter absorbing in the wavelength region of the acceptor," J. Chem. Phys. **139**, 014107 (2013).

[31] G. J. Daniels and D. L. Andrews, J. Chem. Phys. **117**, 6882–6893 (2002).

[32] T. Wakamatsu and S. Odauchi, "Thermal-changeable complex-refractive-index spectra of merocyanine aggregate films," Appl. Opt. **42**, 6929–6933 (2003).

[33] D. J. Segelstein, "The complex refractive index of water," Thesis, University of Missouri-Kansas, USA, 1981.

[34] D. S. Bradshaw and D. L. Andrews, "Optically controlled resonance energy transfer: Mechanism and configuration for all-optical switching," J. Chem. Phys. **128**, 144506 (2008).

[35] D. S. Bradshaw and D. L. Andrews, "All-optical switching based on controlled energy transfer between nanoparticles in film arrays," J. Nanophoton. **3**, 031503 (2009).

[36] T. Meier, Y. Zhao, V. Chernyak, and S. Mukamel, "Polarons, localization, and excitonic coherence in superradiance of biological antenna complexes," J. Chem. Phys. **107**, 3876–3893 (1997).

[37] O. Kuhn and V. Sundstrom, "Pump-probe spectroscopy of dissipative energy transfer dynamics in photosynthetic antenna complexes: A density matrix approach," J. Chem. Phys. **107**, 4154–4164 (1997).

[38] A. Acocella, G. A. Jones, and F. Zerbetto, "What is adenine doing in photolyase?," J. Phys. Chem. B **114**, 4101–4106 (2010).

[39] A. Ishizaki and G. R. Fleming, "On the interpretation of quantum coherent beats observed in two-dimensional electronic spectra of photosynthetic light harvesting complexes," J. Phys. Chem. B **115**, 6227–6233 (2011).

[40] N. Singh and P. Brumer, "Electronic energy transfer in model photosynthetic systems: Markovian vs. non-Markovian dynamics," Faraday Discuss. **153**, 41–50 (2011).

[41] J. M. Jean, C.-K. Chan, G. R. Fleming, and T. G. Owens, "Excitation transport and trapping on spectrally disordered lattices," Biophys. J. **56**, 1203–1215 (1989).

[42] E. K. L. Yeow, K. P. Ghiggino, J. N. H. Reek, M. J. Crossley, A. W. Bosman, A. P. H. J. Schenning, and E. W. Meijer, "The dynamics of electronic energy transfer in novel multiporphyrin functionalized dendrimers: A time-resolved fluorescence anisotropy," J. Phys. Chem. B **104**, 2596–2606 (2000).

[43] M. Bednarz, V. A. Malyshev, and J. Knoester, "Intraband relaxation and temperature dependence of the fluorescence decay time of one-dimensional Frenkel excitons: The Pauli master equation approach," J. Chem. Phys. **117**, 6200–6213 (2002).

[44]M. Yang, A. Damjanović, H. M. Vaswani, and G. R. Fleming, "Energy transfer in photosystem I of *Cyanobacteria Synechococcus* elongates: Model study with structure-based semi-empirical Hamiltonian and experimental spectral density," Biophys. J. **85**, 140–158 (2003).

[45]B. Valeur and M. N. Berberan-Santos, *Molecular Fluorescence: Principles and Applications*, 2nd ed. (Wiley-VCH, Weinheim, 2013).

[46]L. Stryer and R. P. Haugland, "Energy transfer: A spectroscopic ruler," Proc. Natl. Acad. Sci. U.S.A. **58**, 719–726 (1967).

[47]T.-S. Ahn, N. Wright, and C. J. Bardeen, "The effects of orientational and energetic disorder on Forster energy migration along a one-dimensional lattice," Chem. Phys. Lett. **446**, 43–48 (2007).

[48]J. S. Briggs and A. Eisfeld, "Equivalence of quantum and classical coherence in electronic energy transfer," Phys. Rev. E **83**, 051911 (2011).

[49]O. I. Micic, K. M. Jones, A. Cahill, and A. J. Nozik, "Optical, electronic, and structural properties of uncoupled and close-packed arrays of InP quantum dots," J. Phys. Chem. B **102**, 9791–9796 (1998).

[50]R. Koole, P. Liljeroth, C. M. Donega, D. Vanmaekalbergh, and A. Meijerink, "Electronic coupling and exciton energy transfer in CdTe quantum-dot molecules," J. Am. Chem. Soc. **128**, 10436–10441 (2006).

[51]N. Zaitseva, Z. R. Dai, F. R. Leon, and D. Korl, "Optical properties of CdSe superlattices," J. Am. Chem. Soc. **127**, 10221–10226 (2005).

[52]A. G. Brolo, S. C. Kwok, M. D. Cooper, M. G. Moffitt, C.-W. Wang, R. Gordon, J. Riordon, and K. L. Kavanagh, "Surface plasmon-quantum dot coupling from arrays of nanoholes," J. Phys. Chem. B **110**, 8307–8313 (2006).

[53]D. B. VanBeek, M. C. Zwier, J. M. Shorb, and B. P. Krueger, "Fretting about FRET: Correlation between K and R," Biophys. J. **92**, 4168–4178 (2007).

[54]T. Sen, S. Sadhu, and A. Patra, "Surface energy transfer from rhodamine 6G to gold nanoparticles: A spectroscopic ruler," Appl. Phys. Lett. **91**, 043104 (2007).

[55]R. S. Swathi and K. L. Sebastian, "Resonance energy transfer from a fluorescent dye molecule to plasmon and electron-hole excitations of a metal nanoparticle," J. Chem. Phys. **126**, 234701 (2007).

[56]A. Munoz-Losa, C. Curutchet, B. P. Krueger, L. R. Hartsell, and B. Mennucci, "Fretting about FRET: Failure of the ideal dipole approximation," Biophys. J. **96**, 4779–4788 (2009).

[57]S. V. Koushik, P. S. Blank, and S. S. Vogel, "Anomalous surplus energy transfer observed with multiple FRET acceptors," PloS ONE **4**, e8031 (2009).

[58]S. Chatterjee, J. B. Lee, N. V. Valappil, D. Luo, and V. M. Menon, "Investigating the distance limit of a metal nanoparticle based spectroscopic ruler," Biomed. Opt. Express **2**, 1727–1733 (2011).

[59]W. R. Algar, M. G. Ancona, A. P. Malanoski, K. Susumu, and I. L. Medintz, "Assembly of a concentric Förster resonance energy transfer relay on a quantum dot scaffold: Characterization and application to multiplexed protease sensing," ACS Nano **12**, 11044–11058 (2012).

[60]J. R. Walker, "FRETting over the spectroscopic ruler," Science **339**, 1530–1531 (2013).

[61]G. D. Scholes, G. R. Fleming, A. Olaya-Castro, and R. van Grondelle, "Lessons from nature about solar light harvesting," Nat. Chem. **3**, 763–774 (2011).